Leukemia aggressiveness is driven by chromatin remodeling and expression changes of core regulators

Gracia Bonilla[1,2], Alexander Morris[1], Sharmistha Kundu[1,2], Anthony DuCasse[1], Grace Kirkpatrick[1], Nathan E. Jeffries[3,4,5], Kashish Chetal[1], Emma E. Yvanovich[3,4,5], Jelena Milosevic[3,4,5], Ting Zhao[3,4,5], Jun Xia[3,4,5], Rana Barghout[3,4,5], David Scadden[3,4,5], Michael K. Mansour[4,6,7], Robert E. Kingston[1,2], David B. Sykes[3,4,5], Francois E. Mercier[8], Ruslan I. Sadreyev[1,9*]

[1]Department of Molecular Biology, Massachusetts General Hospital, Boston MA, USA; [2]Department of Genetics, Harvard Medical School, Boston MA, USA; [3]Center for Regenerative Medicine, Massachusetts General Hospital, Boston MA, USA; [4]Harvard Stem Cell Institute, Cambridge MA, USA; [5]Department of Stem Cell and Regenerative Biology, Harvard University, Cambridge MA, USA; [6]Division of Infectious Diseases, Massachusetts General Hospital, Boston MA, USA; [7]Department of Medicine, Harvard Medical School, Boston MA, USA; [8]Department of Medicine, McGill University, Montreal, Quebec, Canada; [9]Department of Pathology, Massachusetts General Hospital and Harvard Medical School, Boston MA, USA

* Correspondence should be addressed to:
Ruslan I. Sadreyev
Massachusetts General Hospital
Department of Molecular Biology
Richard B. Simches Research Center
185 Cambridge Street CPZN-7250
Boston MA 02114
sadreyev@molbio.mgh.harvard.edu

ABSTRACT

Molecular mechanisms driving clonal aggressiveness in leukemia are not fully understood. We tracked and analyzed MLL-rearranged leukemic clones independently evolving towards higher aggressiveness. More aggressive subclones lost their growth differential ex vivo but restored it upon secondary transplantation, suggesting molecular memory of aggressiveness. Development of aggressiveness was associated with clone-specific gradual modulation of chromatin states and expression levels across the genome, with a surprising preferential trend of reversing the earlier changes between normal and leukemic progenitors. To focus on the core aggressiveness program, we identified genes with consistent changes of expression and chromatin marks that were maintained in vivo and ex vivo in both clones. Overexpressing selected core genes (Smad1 as aggressiveness driver, Irx5 and Plag1 as suppressors) affected leukemic progenitor growth in the predicted way and had convergent downstream effects on central transcription factors and repressive epigenetic modifiers, suggesting a broader regulatory network of leukemic aggressiveness.

INTRODUCTION

Therapeutic challenges in treating acute myeloid leukemia (AML) often arise from disease heterogeneity and clonal evolution during disease development [1,2] and post-treatment relapse [3,4]. Clonal evolution in leukemia is driven by both genetic and epigenetic changes in hematopoietic stem cells and leukemic progenitors [1,5]. Epigenetic dysregulation is a major component of AML origin and development. Genome-wide dynamics of DNA methylation [6] linked to methylases [7] and demethylase proteins [8] are associated with AML progression and outcome. COMPASS and SWI-SNF chromatin modifiers[9] that include MLL and other protein components [10,11], COMPASS-associated Menin-LEDGF complex [12], and COMPASS antagonists, Polycomb repressive complexes [13–15] are involved both in the origin and further development of AML. Another COMPASS antagonist, histone demethylase Kdm5b is a strong suppressor of AML aggressiveness[15]. Despite clinical and functional evidence of a central role that DNA and chromatin modifiers play in the evolution and maintenance of leukemia, understanding of epigenetic evolution among individual AML clones has remained elusive, in large part due to the heterogeneity of both molecular lesions and phenotypes across individual subclones [1,2,5,16,17].

Addressing these limitations, we analyzed a tractable clonal model to understand the dynamics of chromatin regulation and gene expression during the development of aggressiveness and to identify candidate drivers and suppressors of this process. We used a well-established mouse model of AML driven by the MLL-AF9 fusion [18], a prevalent MLL rearrangement observed in AML patients [19]. We performed genome-wide profiling of chromatin modifications and gene expression in independent MLL-AF9 leukemic clones and characterized epigenomic and transcriptional changes as the cells became more aggressive. Compared to the changes between normal progenitors and the early stage of leukemic development, these aggressiveness-associated

changes affected fewer genes and enhancers and were more clone-specific, consistent with heterogeneity of clonal evolution. These changes often involved gradual shifts of expression levels and chromatin states rather than on/off switching between full silencing and activity. Surprisingly, most of these shifts reversed the prior promoter and enhancer changes observed at the early leukemic stage.

To identify candidate regulators of aggressiveness and its memorization throughout long-term ex vivo culture, we focused on the core set of genes whose in vivo expression and ex vivo chromatin changes were consistent between individual clones. Three genes were further validated, one as a causal driver (Smad1) and two as suppressors of clonal growth (Irx5, Plag1). Mechanistically, we found an unexpected convergence of their downstream transcriptional effects on a group of transcription and epigenetic factors that may represent a broader regulatory network of clonal aggressiveness. Our results show how a dynamic epigenome can enable clonal selection through a shared program conferring growth advantage to aggressive leukemic clones.

RESULTS

Chromatin and gene expression profiling at two stages of leukemia aggressiveness

We employed a cellular model of developing leukemic aggressiveness using the mouse AML model driven by the human MLL-AF9 (KMT2A-MLLT3) fusion protein [18], a recurrent MLL rearrangement [19]. In this model, the leukemic initiation is mainly attributed to MLL fusion driving the dysregulated reprogramming of committed granulocyte macrophage progenitors (GMPs) into leukemic stem cells (LSCs) [18,20]. To track individual leukemic clones, GMPs isolated from CD45.1 congenic mouse were transduced with four individual fluorescent proteins. An equal mix of labeled clones was transplanted into irradiated host mice, followed by longitudinal tracking in bone marrow and blood

for 120 days (Figure 1A). Following engraftment, these clones evolved in bone marrow, resulting in cell-autonomous differences in growth rate. The more aggressive clones 'won' the competition and dominated the bone marrow and peripheral blood.

Winning clones dramatically increased growth rate in vivo as they transitioned from early to aggressive stage (Figures 1A, S1A,B). This difference between the early and aggressive subclones was significantly diminished ex vivo (Figures S1C,D), suggesting the essential role of the bone marrow microenvironment in maintaining aggressive growth. This difference, however, was restored upon secondary re-transplantation (Figures 1A, S1E,F), suggesting an intrinsic cellular memory of aggressive status that was maintained over multiple cell divisions ex vivo. To understand the epigenetic and transcriptional regulation of clonal aggressiveness, we focused on two independent leukemias that evolved into aggressive subclones (Figure 1A). We performed RNA-seq profiling of gene expression in LSC-enriched cell populations at the early and aggressive stages of the same clone both in vivo and ex vivo, as well as ChIP-seq profiling of H3K4me1, H3K4me3, H3K27ac, and H3K27me3 chromatin marks ex vivo. LSC-enriched progenitors from healthy mice were profiled as a normal comparator (Figure 1A).

Early changes of promoter chromatin marks and gene expression are consistent between leukemic clones

As an example of a major driver of MLL-rearranged (MLLr) leukemias[21], *Meis1* gene was strongly activated in all leukemic subclones when compared to normal progenitors, as evidenced by transcriptional upregulation, concomitant with the loss of repressive chromatin mark H3K27me3 and gain of active marks H3K27ac and H3K4me3 at the promoter (Figures 1B, C). However, this activation of *Meis1* and other major leukemic drivers did not change in aggressive subclones

(Figures 1B,C, S1G-K), suggesting that their further upregulation is not required for clonal aggressiveness.

Genome-wide, most changes of promoter chromatin marks and gene expression between normal progenitors and the early leukemic stage were also consistent between clones and maintained throughout leukemia progression (Figures 1D, S1L). When compared to normal progenitors, the two early-stage leukemic clones shared the vast majority (~85%) of differentially expressed genes (DEGs, Supplementary Data 1) and large fractions of promoters with H3K27ac, H3K4me3, and H3K27me3 changes (Figure 1E). According to EnrichR [22] pathway analysis, DEGs shared between clones were enriched in IL2/STAT5 and EMT pathways and targets of central transcription factors (Myc, Hif1a, Sox2, Tcf3, Mecom, Af4, Runx1, Cebpa, Irf8, p53, Smad3) and epigenetic factors (p300, Brd4, Polycomb proteins, Dnmt1) implicated in hematopoiesis and leukemogenesis (Figure 1F).

Compared to normal progenitors, promoter H3K27ac was preferentially increased and H3K7me3 was preferentially decreased, whereas H3K4me3 changes were more balanced (Figure 1G). Global gene expression was modestly skewed towards upregulation (Figure 1G). The combination of chromatin marks was robustly predictive of expression changes, with active marks H3K27ac and H3K4me3 being the strongest predictors (Figure S1M), despite a substantial part of promoter chromatin remodeling did not manifest as expression changes, for example at transcriptionally silent promoters that underwent H3K27me3 decrease without increasing active H3K4me3 and H3K27ac marks (Figure 1D, middle part of the heatmap).

When compared to normal progenitors, both stages of aggressiveness had similar differences in promoter chromatin marks (Figure 1H, points near diagonal); the minority of promoters that deviated between early and aggressive subclones (Figure 1H, points away from diagonal) are the focus of our analyses.

Promoter H3K4me3 and H3K27me3 levels define three distinct chromatin states

To understand global patterns of promoter remodeling, we analyzed genome-wide relationships between promoter chromatin marks. We focused on H3K4me3 and H3K27me3, given their roles in promoter regulation [23] and the importance of the corresponding COMPASS/MLL [10,11] and Polycomb protein complexes [13–15] in leukemia. The scatterplot in Figure 1I represents the combination of H3K27me3 (x axis) and H3K4me3 levels (y axis) at each promoter in normal progenitor cells as a point colored by the level of gene expression. The two marks followed a distinct pattern previously observed elsewhere [24]. They were anticorrelated among active promoters (the upper branch of the plot), where the fully active chromatin state [25] with thehighest H3K4me3 and no H3K27me3 was located at the tip of this branch (Figure 1I, red circle). H3K4me3 and H3K27me3 were positively correlated and co-depleted among silent promoters (the lower branch of the plot). The lowest tip of this branch corresponded to a full H3K4me3 and H3K27me3 depletion (Figure 1I, blue circle), which typically associates with constitutive heterochromatin and DNA methylation [25]. The “nexus” between these two branches included promoters with the highest H3K27me3 and moderate H3K4me3 (Figure 1I, orange circle), corresponding to Polycomb-repressed bivalent chromatin state that isoften associated with repressed developmental factors poised for activation [25,26]. This overall pattern of three chromatin states connected by two branches was similar in leukemic clones (Figures S1N). However, many major leukemic drivers were bivalent in normal progenitors but were activated along the active branch in leukemia (Figures 1B,C, S1G-J).

Genome-wide trends of promoter chromatin remodeling in early leukemic progenitors

We used this genome-wide pattern of chromatin states to analyze the chromatin state shifts between normal and early leukemic progenitors. In Figure 1I these shifts are depicted as arrows with the approximate numbers of promoters following each direction. Different directions were associated with targets of different transcription factors and chromatin modifiers, suggesting specific roles of these factors in promoter regulation (Figure S1O). The strongest trend involved preferential movements from active and bivalent states (Figure 1I, red and orange circles) towards the silent state [25] (blue circle), corresponding to chromatin silencing and consistent with the known leukemic role of de novo DNA methylation [7]. The second trend involved movements from bivalent state (Figure 1I, orange circle) towards active state (red circle) via H3K4me3 increase and H3K27me3 decrease accompanied by transcriptional upregulation (Figures S2D-F). Notably, this trend included major leukemic drivers (Hoxa9, Meis1, Six1, Six4, Eya1, etc., Figures 1B,C, S1G-K). The third, unexpected trend involved a subset of bivalent promoters that increased H3K4me3 while maintaining high H3K27me3 (Figure 1I, upward arrow on the right) and the initial transcriptional repression (Figure S2A-C), suggesting that these changes of H3K4 methylation were uncoupled from the changes of Polycomb repression. Taken together, we identified recurrent shifts between promoter chromatin states driven by specific changes in the global activity of repressive and activating epigenetic factors.

Enhancer chromatin remodeling in early leukemic progenitors was consistent between clones

We identified ~40,000 enhancer elements based on the density of H3K27ac or H3K4me1 and the absence of strong H3K4me3 enrichment, and analyzed the shifts of enhancer chromatin states

between normal and early leukemic progenitors. As an example, two enhancers in the proximity of the *Des* gene showed consistent increases in H3K27ac and H3K4me1 in both clones (Figure 1J). These changes are quantified in a scatterplot (Figure 1K, top) where individual points correspond to the combination of two marks in normal (grey), early leukemic (blue), and aggressive cells (red), with proximal gene expression shown as a barplot. *Pitx2* (Figure 1K, middle, and Figure S1P) and *Lmo1* proximal enhancers (Figure 1K, bottom, and Figure S1Q) also underwent consistent activation and deactivation of chromatin state. Across the genome, 17,338 enhancers changed H3K27ac or H3K4me1 >2-fold in at least one clone (Figures 1L, S1R). These changes correlated between the two marks and were consistent between two clones (Figure 1L), which shared the majority of enhancers with >2-fold change of H3K27ac and a large fraction of enhancers with >2-fold change of H3K4me1 (Figure 1M). The magnitude of these changes was largely maintained at the aggressiveness stage (Figure 1N); the minority of enhancers that showed stage-specific differences are the focus of our analyses below.

H3K27ac and H3K4me1 levels across enhancers were largely correlated (Figure 1O). At the early leukemic stage, global changes of H3K27ac were balanced between increases and decreases, and this balance was a result of two opposite trends: concomitant H3K27ac and H3K4me1 changes skewed towards increase (Figures 1O and S9, diagonal arrows), and H3K27ac changes alone (decoupled from H3K4me1) which were skewed towards decrease (Figures 1O and S1S,T, vertical arrows). Interestingly, H3K4me1 changes were skewed towards increase regardless of whether they were coupled to H3K27ac changes (diagonal arrows) or not (horizontal arrows), suggesting a global increase of enhancer H3K4 methylation independent from H3K27 acetylation.

Clonal aggressiveness is accompanied by promoter chromatin and gene expression changes

We focused on chromatin and expression changes associated with clonal aggressiveness. The *Fhdc* promoter, for example, was in a repressed bivalent state in normal progenitors, with no H3K27ac, high H3K27me3, and modest H3K4me3. At the early leukemic stage in both clones, it switched to a transcriptionally active state with high H3K4me3 and H3K27ac and no H3K27me3 (Figure 2A). However, at the aggressive stage this change was partially reversed by shifting back the levels of chromatin marks and expression. The *Fyb* promoter was active in normal progenitors, with high H3K27ac and H3K4me3 and no H3K27me3. At the early leukemic stage in both clones, it shifted to a repressed bivalent state with low or no expression. At the aggressive stage, this strong repression was partially reversed via decreasing H3K27me3 and increasing H3K4me3 and H3K27ac (Figure 2B). These changes are quantified in the scatterplots of H3K27me3 vs H3K4me3 (Figure 2C), with additional examples in Figures S3A-F. Collectively, these changes suggest that developing clonal aggressiveness largely involved modulation of promoter activity on a continuous scale rather than on/off switching between extreme chromatin states.

MLL-AF9 direct targets are stable during aggressiveness development

To address whether clonal aggressiveness could be ascribed to increased activity of direct MLL-AF9 targets, we analyzed target promoters with the strongest MLL-AF9 peaks (Homer score ≥ 13) based on published ChIP-seq data in mouse MLL-AF9 HSPCs [27]. Most targets were active in both normal and leukemic progenitors. At the early leukemic stage 35-40% of MLL-AF9 targets (depending on the clone) were further upregulated, while only 5-6% were downregulated, summarized as heatmap (Figure S3G) and trends of combined H3K27me3 and H3K4me3 changes (Figure S3H,I). However, there was no preferential activity shift at the aggressive stage, where only

a small minority of MLL-AF9 targets were differentially expressed (12-15% depending on the clone) and were mostly downregulated (Figure S3J). Only 3.5-12% of MLL-AF9 targets underwent H3K4me3, H3K27ac, or H3K27me3 changes at the aggressive stage (Figure S3J).

Remarkably, virtually all MLL-AF9 targets that were initially repressed by Polycomb and had high H3K27me3 in normal progenitors underwent a dramatic H3K27me3 depletion and H3K4me3 increase at the early leukemic stage (diagonal arrow towards upper left in Figure S3H,I). These targets included major leukemogenic drivers Hoxa9, Meis1, Six1, Six4, etc (Figures 1B, S1G-K). However, neither their expression nor chromatin state changed further at the aggressive stage (Figures 1B,C, S1G-I), with the possible exception of Eya1 and Jmjd1c that changed expression in one of the clones (Figures S1J,K). This absence of clone-consistent changes suggested that direct regulation by MLL-AF9 or by major leukemogenic drivers was unlikely to be a primary driver of clonal aggressiveness.

Clone specific changes during development of aggressiveness preferentially reversed early leukemic changes

We then analyzed global patterns of aggressiveness-associated changes in gene expression and promoter chromatin marks (Figures 2D, S3K). These changes affected many promoters across the genome, although fewer than at the early leukemic stage (Figure 1D). This smaller but substantial magnitude of aggressiveness-associated changes was also evident from principal component analysis (PCA) of gene expression (Figure 2E). The difference between normal progenitors (gray points) and all leukemic subclones regardless of aggressiveness (blue and red) corresponded to the first principal component (x axis) that accounted for the majority (64%) of overall expression variation. The difference between two stages of aggressiveness (blue vs red) corresponded to

principal component 2 (y axis) and accounted for a smaller but substantial fraction of overall variation (20%).

Compared to the highly consistent changes at the early leukemic stage (Figure 1D), changes at the more aggressive stage (Figure 2D) were more clone-specific, suggesting distinct paths to the acquisition of aggressiveness. Clones 1 and 2 shared 54% and 67% (n=1388) of aggressiveness-associated DEGs, respectively (Figure 2F, Supplementary Data 1), compared to ~85% at the early stage (Figure 1E). This clonal specificity was even more pronounced among chromatin marks (Figure 2F).

Genes with consistent expression changes at the aggressive stage in both clones (Figure 2G) were enriched in central regulatory pathways (EMT, interferon and inflammatory responses, IL6/JAK/STAT3, IL2/STA5, KRAS signaling), targets of transcription factors (Satb1, Cebpa, Myc, E2f8, Mecom, Gata1/2, Stat1, Jun, Irf4/8, Smad3/4, p53, Sox2, Oct4/Pou5f1, etc), chromatin modifying proteins (Polycomb components, Dot1l, p300, Arid3b, Setdb1), and DNA methylation and demethylation machinery (DNMT1, Tet1). These factors included general cell cycle regulators (e.g. E2f8), pluripotency factors (Sox2, Oct4, etc), and regulators of leukemic growth (Cebpa, Myc, Dot1l, etc). Among chromatin modifiers, there was a notable enrichment across Polycomb group proteins (Rnf2, Kdm2b, Suz12, Eed, Ezh2, Jarid2, MTF2), suggesting a major role of Polycomb in transcriptional regulation of aggressiveness.

The majority of DEGs associated with aggressiveness (~70-75% depending on the clone) were already differentially expressed at the prior early leukemic stage (Figures 2H, S3L). Promoters affected by chromatin remodeling also had a strong ~50% overlap between two stages (Figures

2H, S3L). Surprisingly, most of these changes at the aggressive stage were not a further amplification of the early leukemic changes but their reversal (Figures 2I, S3M; large arrows depict the early changes compared to smaller arrows that depict changes at the aggressive stage).

Consistent with a strong influence of the bone marrow environment, gene expression changes between the early and aggressive subclones in vivo were different from the changes ex vivo. DEGs observed in vivo and ex vivo shared only 20% of genes upregulated and 13% of genes downregulated at the aggressive stage (Figure S3N). We postulated that these shared genes included potential mediators of cellular memory that was maintained despite the diminished growth difference between early and aggressive subclones ex vivo (Figure S1C,D) and manifested upon secondary re-transplantation (Figure S1E,F).

For each individual subclone, expression patterns ex vivo and in vivo had extensive differences. The sets of these condition-specific DEGs were similar for the early and aggressive subclones of the same clone, with >50% overlap but still notable differences (Figure S3O). Accordingly, the early and aggressive subclones had largely overlapping but different functional gene categories enriched among these DEGs (Figure S3P). The shared gene categories included MYC targets, cholesterol homeostasis, and p53 pathways enriched among downregulated genes. Categories unique to the early stage included E2F1, XRN2 targets and mTORC1 pathway among downregulated genes and inflammation-associated pathways among upregulated genes. Categories unique to the aggressive stage included LXR, KDM2B, ZFP281, and TCF7 targets enriched among downregulated genes (Figure S3P).

Genome-wide trends of promoter chromatin remodeling in aggressive progenitors

Trends of concomitant H3K4me3 and H3K27me3 changes at the aggressive stage (Figures 2J, S3Q) were different from the early leukemic changes (Figure 1I). Despite a stronger clone specificity, three preferential directions were consistent between two clones (yellow arrows in Figures 2J, S3Q). Promoters with high H3K27me3 preferentially increased H3K4me3 (Figures 2J, S3Q, vertical upward arrow on the right), similar to the early stage (Figure 1I). However, among promoters depleted in H3K27me3, the early skew towards H3K4me3 decrease (Figure 1I, vertical downward arrow on the left) was dramatically reversed to a preferential H3K4me3 increase (Figures 2J, S3Q, vertical arrow on the left). Finally, bivalent promoters (Figures 2J, orange circle) shifted preferentially towards active state (red circle) via H3K4me3 increase and H3K27me3 decrease (upward diagonal arrow), consistent with a strong enrichment of Polycomb targets among aggressiveness associated DEGs (Figure 2F). This trend was similar to the early leukemic stage (Figure 1I), although this activation involved virtually no MLL-AF9 targets, which were stably active. Collectively, all these trends involved H3K4me3 increase in various chromatin contexts, suggesting a major role of H3K4 methylation and consistent with the recent report of H3K4me3 demethylase Kdm5b as a potent suppressor of leukemic aggressiveness[15].

Chromatin changes were correlated with gene expression; the combination of promoter H3K4me3, H3K4me1, H3K27ac, and H3K27me3 differences ex vivo was robustly predictive of expression differences (R=0.5, Figure S3R). Active mark H3K27ac was the most predictive, followed by H3K27me3 and H3K4me3(Figure S3R, heatmap on the right). Despite the difference between expression changes observed in vivo and ex vivo, a subset of DEGs was maintained throughout ex vivo culturing (Figure S3N). Accordingly, despite chromatin mark changes ex vivo were less predictive of the expression changes in vivo (Figure S3S), active marks H3K27ac and H3K4me3 were still among the most predictive (Figure S3S, heatmap on the right).

Aggressive subclones preferentially activated chromatin state at enhancers and reversed early leukemic changes

Aggressiveness was associated with widespread modulation of enhancer chromatin marks. As an example, the Net1 enhancer increased both H3K27ac and H3K4me1 at the aggressive stage (Figure 3A), whereas the enhancer upstream of gene Zfp516 decreased both marks (Figure 3B, see additional examples in Figure S4A-C). These changes are quantified as scatterplots of H3K4me1 vs H3K27ac at the same enhancer in Figures 3C, S4A-F . Similar to promoters (Figures 2A-C, S3A-F), chromatin mark levels at these enhancers were gradually modulated, as opposed to switching between extreme chromatin states. Globally, aggressiveness-associated changes of enhancer chromatin state showed a strong skew towards activation (Figures 3D, S4G). The consistency of H3K27ac and H3K4me1 changes between two clones was significant (20-22% for H3K27ac and 11-15% for H3K4me1 depending on the clone, Figure 3E) but lower than the clonal consistency of chromatin mark changes at promoters (Figure 2F).

Like promoters (Figure 2H), a large proportion of enhancers affected by the development of aggressiveness already underwent changes at the early leukemic stage. This proportion was especially large for H3K27ac (Figures 3F, S4H). Surprisingly, most of these enhancers reversed their initial H3K27ac changes (Figures 3G, S4I; large arrows depict changes at the early stage compared to smaller arrows depicting changes at the aggressive stage).

Taken together, these aggressiveness-associated changes of gene expression and chromatin marks at promoters (Figures 2A,B,H,I) and enhancers (Figures 3A,B,F,G) suggest a few important observations. First, most of these changes were gradual quantitative shifts rather than binary

switches between silent and active states. These gradual shifts were often consistent between clones to a considerable degree of quantitative detail. Second, most of these shifts were preceded by the prior changes of the same promoter or enhancer at early leukemic stage. When compared to normal progenitors, these genes most often maintained the early direction of shift, either activation or repression, but altered the magnitude of this change (Figure 1H,N). This suggests that increasing clonal aggressiveness involved quantitative adjustment of initial dysregulation that occurred during leukemogenesis. Unexpectedly, this quantitative adjustment often dampened the initial perturbation. As one possible explanation of clonal fitness advantages conferred by this dampening, some of the extremely strong downstream effects of initial leukemogenic lesion (MLL rearrangement) may require fine tuning or even toning down for further increase of cell growth and survival. This fine tuning might be mediated via additional mutagenesis, changes in expression of key transcription factors, chromatin remodeling by epigenetic factors, or other mechanisms.

Genome-wide trends of enhancer chromatin remodeling in aggressive progenitors

In leukemic cells (Figures 3H, S4J), like in normal progenitors (Figure 1O), H3K27ac and H3K4me1 levels were correlated across all enhancers. The trends of concomitant H3K27ac and H3K4me1 changes were consistent between two independent aggressive clones. H3K27ac changes were skewed towards increase (Figures 3H, S4J) in contrast with more balanced changes at the early stage (Figure 1O), mostly due to the reversal of preferential H3K27ac changes uncoupled from H3K4me1 change (vertical yellow arrow). These changes were skewed towards decrease at the early leukemic stage (Figure 1O, vertical arrows) but switched towards increase at the aggressive stage (Figures 3H and S4J). This suggests that in addition to continued global increase of enhancer H3K4me1, aggressiveness was associated with increase of H3K27 acetylation often uncoupled from H3K4 methylation.

These changes of enhancer chromatin marks were associated with various transcription factor binding motifs according to MEME[28] (Figure 3I). Transcription factors associated with the coordinated changes of both H3K27ac and H3K4me1 included ETS family proteins and related PU.1 factor that have been implicated in hematopoiesis and leukemogenesis [29,30]; CEBPB/D/E/G involved in myeloid hematopoiesis and aggressive leukemia [31–33]; and ZNF384 with reported leukemic fusions and regulation of hematopoietic stem cell factors[34]. Motifs associated with only H3K27ac changes involved major regulatory factors STAT2, BCL11B, IKZF1, NR5A1/2, and KLF9, whereas H3K4me1 changes were associated with leukemic regulators CEBPA, MYB, RUNX1, pluripotency factor KLF4, AP-1 factor JUN, and other factors (Figure 3I). Taken together, enhancer chromatin remodeling at the aggressive stage was associated with motifs for ETS, CEBP, AP-1 factors and other differentiation and leukemic regulators.

For each enhancer, we calculated correlation between its H3K27ac level and the expression of the proximal gene across the five profiled cell types (normal progenitors and two stages of aggressiveness in two independent leukemic clones). As an example, Figure 3J quantifies this correlation for two enhancers depicted in Figures 3A,B. Among all enhancers with aggressiveness-associated H3K27ac changes, there was a remarkable skew towards high correlation with proximal gene expression (histogram in Figure 3K), suggestive of transcriptional regulation. We focused on 406 enhancers with the highest correlation to gene expression (Pearson R>0.7, right of the dotted line in Figure 3K). EnrichR analysis of the corresponding 307 genes (Figure 3L) revealed strong enrichment in the targets of major differentiation, hematopoiesis, and leukemogenesis regulators (Wt1, Esr1, Lmo2, Gf1, Myb, Tal1, Cebpd, Stat3, Meis1), components of super-elongation complex also known as MLL fusion partners (Af4/Mllt3 and Af9/Enl), pluripotency factors (Sox2, Nanog,

Pou5f1, Prdm14), and chromatin modifiers (Brd4, p300, Smarcd1, Setdb1) often implicated in hematopoiesis and leukemia. The enrichment of Nfkb1 and Smad3/4 targets suggested the involvement of NFKB and TGFβ pathways. Although many enriched categories were similar to the ones among the whole population of aggressiveness-associated genes (Figure 2G), there were notable differences. Polycomb components were not as strongly enriched (Figure 3L), suggesting lesser Polycomb control; whereas targets of Kdm5b and Smad1 were enriched exclusively among enhancer-correlated promoters, suggesting that Kdm5b, H3K4 histone demethylase known to suppress AML aggressiveness[15] and Smad1, a BMP pathway effector, are involved in enhancer-mediated gene regulation.

Core genes defined by consistent aggressiveness-associated expression and chromatin changes in vivo and ex vivo

Despite substantial variability by clone and condition, some aggressiveness-associated DEGs were consistent between clones (Figure 2F) and maintained their differential status both in vivo and ex vivo (Figure S3N). To identify potential drivers or suppressors of aggressiveness that persisted ex vivo, we defined a core set of genes with consistent expression and promoter chromatin changes persisting between ex vivo and in vivo conditions in a clone-independent manner (Figure 4A). We identified 17 such genes consistently upregulated and 11 genes consistently downregulated at the aggressive stage (Figures 4B, S5A).

While none of these genes were strong MLLr targets, many were known regulators of hematopoiesis, leukemia and other cancers. Among upregulated genes, Rxra is a hormone receptor mutated and therapeutically targeted in an aggressive form of AML, acute promyelocytic leukemia [35]. Smad1 is a key effector in BMP signaling pathway playing an important role in normal

hematopoiesis [36,37] and leukemia [38,39]. Peg10 is known to enhance tumor growth by driving cell cycle progression through the inhibition of TGFβ pathway [40,41]. Consistent with this mechanism, another upregulated gene Matn2 is activated by TGFβ signaling inhibition [42].

Among downregulated genes, homeobox factor Irx5 plays major roles in early development [43,44], metabolism [45] and cancers [46,47], and is upregulated in AML patients and cell lines [48], but no mechanistic role in AML has been reported. Irx5 is a strong target of MLL-AF9 binding and transcriptional regulation [49] and was dramatically activated at the early leukemic stage (Figures S5A, 4C,D). However, in contrast to most MLL-AF9 targets (Figures S3G-I), Irx5 reversed this activation and was downregulated in aggressive cells (Figure S5A, 4B-D). Plag1 is an oncogene involved in the origin of leukemia [14,50] and was upregulated at the early leukemic stage (Figures S5A,B, 4D). However, similar to Irx5, Plag1 reversed this activation and was downregulated at the aggressive stage (Figures S5A,B, 4B,D). To our knowledge, Plag1 has not been previously implicated in the development of AML aggressiveness. Protein tyrosine phosphatase Ptpn3 is a potential tumor suppressor facilitating the activity of TGFβ pathway by stabilizing TGFβ receptor [51]. Ptpn3 downregulation was in line with the upregulation of Peg10 and Matn2 associated with TGFβ inhibition (Figure 4B). Finally, Igf1r is a major regulator of cell transformation and oncogenesis, including AML [52], consistent with Igf1r upregulation at the early leukemic stage (Figure S5A). However, once MLLr leukemia is established, Igf1r is not anymore required for clonal propagation [52], in line with the observed Igf1r reversal towards downregulation at the aggressive stage (Figures S5A, 4B).

Gradual modulation of core genes involved reversal of early leukemic changes

Compared to normal progenitors, most core genes maintained their activation or repression at both leukemic stages, but its magnitude was stage-specific (Figure S5A). Of note, enhancers proximal to these genes often had similar gradual shifts of chromatin state. As an example, strong Polycomb repression of *Irx5* promoter in normal progenitors was completely removed at the early leukemic stage but partially reversed at the aggressive stage by increasing H3K27me3 to a moderate level while partially decreasing H3K4me3 and H3K27ac (Figure 4C, left). This partial reversal of early activation was paralleled by H3K27ac and H3K4me1 changes at a proximal enhancer (Figure 4C, right). This reversal is quantified in Figure 4D as scatterplots of promoter H3K27me3 vs H3K4me3 (left) and enhancer H3K4me1 vs H3K27ac (middle), along with gene expression changes (barplots on the right). *Plag1* had even a stronger reversal of early promoter and enhancer activation, which resulted in an almost complete return to the chromatin state and expression observed in normal progenitors (Figures S5B, 4D). This return suggests that despite the known oncogenic role of Plag1 [14,50], its upregulation may paradoxically be absent in patients with advanced AML.

Conversely, promoters and proximal enhancers of *Smad1* (Figure 4E) and *Rxra* (Figure S5C) were active in normal progenitors, followed by strong repression at the early leukemic stage and its partial reversal at the aggressive stage. These changes are quantified in Figure 4F. As RXRA is a well-known leukemogenic driver in a different genetic background of PML-RARA fusion [35], its behavior in aggressive MLL-AF9 clones may suggest a more general role in driving leukemic aggressiveness, uncoupled from its leukemogenic role.

The fraction of the core genes that were already affected at the early stage (Figures 4G, S5D) was even larger than among the broader set of all aggressiveness-associated promoters (Figures 2H, S3L). Most of these promoters reversed their early leukemic changes of gene expression and

chromatin marks (Figure 4H, S5E), contrary to the naïve expectation that these changes would be further amplified.

Functional validation of aggressiveness-associated gene candidates

Three core aggressiveness-associated genes: Irx5, Plag1, and Smad1 were selected for validation in leukemic progenitors. This selection was based on the degree and clonal consistency of chromatin mark and expression changes during clonal progression (Figures 4B,C-F). Since transcription factors Irx5 and Plag1 were consistently repressed at the aggressive stage (Figures 4C,D, S5B), we hypothesized that they were suppressors of aggressive leukemic growth. Since BMP pathway effector Smad1 was consistently activated (Figures 4E,F), we hypothesized that Smad1 is a driver of aggressive leukemic growth.

To validate phenotypic effects of Irx5, Plag1, and Smad1, we used lentiviral transduction to overexpress these genes in leukemic progenitor clones. Irx5 and Plag1 were overexpressed in aggressive leukemic progenitors to test their suppressive effect while Smad1 was overexpressed in leukemic progenitors at the early leukemic stage to test its activating effect. As a positive control, the known oncogenic driver, Kras G12V mutant [53], was overexpressed in leukemic progenitors at the early stage. Expression was confirmed at the RNA level (Figure 5A). Overexpression of these genes had a strong effect on cell growth (Figure 5B). Smad1 overexpression increased growth rate by 45% (decreased the doubling time from 13.7 to 9.5 hours), even more than Kras G12V expression (decreased the doubling time from 13.7 to 11.7 hours). The overexpression of Irx5 and Plag1 in an aggressive clone had strong effects in the opposite direction, suppressing growth rate by 62% (increase of doubling time from 10.1 to 26.2 hours) and 48% (increase of doubling time from 10.1 to 19.3 hours), respectively (Figure 5B).

The size and morphology of leukemic cells overexpressing either of these genes were similar to non-transduced control cells by Wright-Giemsa staining (Figure 5C). We also assessed effects of gene overexpression on colony formation using a growth in methylcellulose assay (Figures 5D,E). The aggressive subclone had similar colony formation capacity to the early subclone, and gene overexpression did not have a dramatic effect on the numbers of formed colonies (Figure 5D). However, these genes had different specific effects on the colony growth (Figure 5E). Aggressive cells, as opposed to the early subclone, often had a pattern of spreading within the colony. Irx5 or Plag1 overexpression strongly reduced this spreading. Irx5 overexpression led to visually lower cell numbers per colony, consistent with a strong decrease of cell growth. Kras overexpression in the early subclone strongly increased the pattern of spreading. Smad1 overexpression did not increase this spreading but produced much denser colonies with visually more cells per colony, consistent with a strong increase of cell growth.

The early progenitor marker IL-3R (CD123) and markers of mature myeloid cells Gr-1 and CD11b remained stable when compared to non-transduced leukemic progenitors (Figures 5F, S6A-C), suggesting no changes in myeloid lineage. To understand the effects on leukemia initiating cell potential, we quantified the intensity of c-Kit (CD117) staining (Figures 5F,G). Aggressive subclone had a decreased stem cell potential compared to the early clone (22% vs 73%). In the early subclone, Smad1 overexpression further increases stemness from 73% to 97%, whereas Kras overexpression decreases stemness from 73% to 29%. In the aggressive subclone, Irx5 overexpression causes only a modest change of stemness from 22% to 25%, whereas Plag1 overexpression increases stemness from 22% to 70% (Figure 5G).

To analyze the effects on cell cycle, we performed flow cytometry using propidium iodide DNA staining in transduced and non-transduced progenitors (Figures 5H, S6D,E). The overexpression of Smad1, Irx5, and Plag1 resulted in only modest shifts between the phases of cell cycle. In the early subclone, Smad1 overexpression decreased S-phase fraction by 5%, from 48% to 43%, and increased G1 fraction by 5%, from 39% to 44%, suggesting a moderate extension of G1 at the expense of S-phase. In the aggressive subclone, both Irx5 and Plag1 overexpression produced similar small shifts towards the extension of G1-phase and decrease of S-phase (Figures 5H, S6D,E).

To quantify apoptosis, we performed flow cytometry of transduced and non-transduced leukemic progenitors using Annexin V staining in combination with the DAPI cell viability dye (Figure 5I). The fraction of apoptotic (Annexin+ / DAPI-) cells was small, with the lowest fraction of ~2% apoptotic cells observed in non-transduced aggressive subclone and in Kras-overexpressing early subclone, and the highest fraction of ~7% apoptotic cells observed in Irx5-overexpressing aggressive subclone. These modest differences were consistent with the effects of Kras and Irx5 on cell growth, although the absolute fractions of apoptotic cells were low and therefore unlikely to fully account for the observed growth effects.

Finally, we tested the effects of pharmacological inhibition of Smad1 activity using an existing small molecule inhibitor of the ALK2/BMP pathway, LDN-212854 [54]. An *in vitro* viability assay was performed by treating (1) early clones, (2) aggressive clones of leukemic progenitors, and (3) a normal non-cancer GMP cell line overexpressing ER-Hoxb8 that maintains cells in a self-renewing GMP state [55]. LDN-212854 suppressed the growth of all three cell lines with an IC_{50} in the micromolar range, with the strongest inhibition observed in the aggressive cells (Figure 5J, IC_{50} of

0.74 uM, 0.57 uM, and 0.44 uM for normal, early, and aggressive progenitors, respectively). Unfortunately, LDN-212854 was highly toxic to mice (6 mg/kg i.p. injections twice daily) and it was therefore not possible to examine the effect of small molecule Smad1 inhibition *in vivo*.

AML patient data supports the clinical relevance of SMAD1, IRX5, and PLAG1

Survival analysis of public TCGA (https://www.cancer.gov/tcga) AML patient dataset implemented in BloodSpot[56] revealed significant association of higher IRX5 expression with longer overall survival (Figure 6A), consistent with Irx5 downregulation in more aggressive mouse progenitors (Figure 4C,D) and cell growth suppression upon Irx5 overexpression (Figure 5B). Consistent with Smad1 upregulation in more aggressive mouse progenitors (Figure 4E,F) and Smad1 effect on cell growth (Figure 5B), higher SMAD1 expression tended to correspond to shorter overall survival (Figure S6F), albeit the difference was not statistically significant. PLAG1 expression did not show significant survival association with patient survival (Figure S6F).

To assess the expression of SMAD1, IRX5, and PLAG1 across various AML subtypes (NPM1, PML-RARA, CEBPA, etc.) we analyzed the BeatAML 2 database [57] expression data in bone marrow of AML patients, grouped by driver mutations and compared to healthy bone marrow controls (Figure 6B). Assuming that the majority of expression signal in AML bone marrow would be coming from aggressive leukemic clones, we compared the expression differences between AML patients and healthy controls to the differences that we observed between aggressive mouse subclones and normal mouse progenitors shown Figures 4D,F.

SMAD1 expression in the BeatAML database is substantially downregulated in MLLr AML patients compared to healthy controls (Figure 6B). This is consistent with our findings in mouse cells, where

SMAD1 was strongly downregulated in early leukemic subclones, and despite a partial reversal of this downregulation in aggressive subclones, SMAD1 expression still remained lower than normal (Figure 4F). In other AML subtypes, however, SMAD1 expression is affected to a smaller extent, possibly suggesting a special role of SMAD1 regulation in MLLr AMLs. In contrast, IRX5 is upregulated in MLLr AMLs (Figure 6B). This is consistent with our findings that IRX5 is strongly upregulated in early mouse leukemic subclones, and although this upregulation is partially reversed in aggressive subclones, the level of IRX5 expression remains higher than normal (Figure 4D). The upregulation of IRX5 is also evident across other major AML subtypes, suggesting a more universal IRX5 regulation in various AMLs (Figure 6B). PLAG1 shows no significant expression change among MLLr AML patients and a modest downregulation in some other AML subtypes (Figure 6B). Our observations in mouse progenitors suggest that PLAG1 is strongly upregulated in early mouse leukemic clones, consistent with previously published evidence of its oncogenic role in AML [14,50]. However, at the aggressive leukemia stage, PLAG1 then undergoes near-complete reversal and returns to a very low expression similar to normal progenitors (Figure 4D). This strong reversal in aggressive subclones may contribute to the lower average expression in the bone marrow of AML patients (Figure 6B).

Our observations in mouse leukemic progenitors were also consistent with SMAD1, IRX5, and PLAG1 expression in human leukemic progenitors from MLLr AML patients profiled with single-cell RNA-seq [16]. SMAD1 was downregulated while IRX5 and, to a smaller extent, PLAG1 were upregulated in leukemic compared to normal GMPs (Figure 6C). The magnitude of these differences was somewhat lower but on a similar scale to the dysregulation of a major leukemic driver HOXA9.

According to the BloodSpot database [56], in normal human hematopoiesis SMAD1 is strongly expressed in HSCs and hematopoietic progenitors but is dramatically downregulated during further myeloid differentiation (Figure 6D). SMAD1 is also downregulated in various AML subtypes, especially MLLr AML (Figure 6D), consistent with Smad1 repression in mouse (Figures 4C,E) and human leukemic progenitors, Figure 6C). IRX5 has low expression levels across human HSCs, progenitors, and differentiated cells and in most AML subtypes except for t(15;17) PML-RARA fusion leukemia where IRX5 is strongly upregulated. PLAG1 is strongly expressed in human HSCs and gradually downregulated through stages of myeloid differentiation. Its expression is relatively low in all AML subtypes profiled in BloodSpot (Figure 6D).

Convergence of Smad1, Irx5, and Plag1 downstream transcriptional effects suggests a common regulatory network

To understand transcriptional effects of Smad1, Irx5 and Plag1 overexpression, we performed RNA-seq and compared genome-wide differential expression patterns (Figure 6E-G, Supplementary Data 2). Consistent with their opposite effects on cell growth (Figure 5B), Smad1 effects were largely opposite to the effects of Plag1 and Irx5 (Figure 6E). These opposite effects were associated with targets of key regulatory proteins (Figure 6F): Polycomb components Kdm2b, Ring1b, Suz12, Ezh2 and Mtf2, central chromatin factors Brd4, Setdb1 and Arid3a, DNA methylation and demethylation components Dnmt1 and Tet1, and major transcription factors (Myc, Myb, Irf8, Ikzf1, Wt1, Rxr, Tal1, Sox2, Nanog, p53, Smad3 etc). There was a significant overlap between individual DEGs affected in the same direction by Irx5 and Plag1 (Figures 6G); for example, both upregulated Bcorl1, a Polycomb component strongly involved in leukemia [58,59] and downregulated Lin28b, which regulates hematopoiesis by transcriptionally inhibiting Polycomb component Cbx2 [60] (heatmap in Figure 6H and schematic in Figure 6I). Notably, Smad1 expression

itself was downregulated by Plag1 overexpression (Figure 6H), suggesting a negative transcriptional regulation of Smad1 by Plag1 (Figure 6I). A significant fraction of Irx5 and Plag1 targets was affected by Smad1 in the opposite direction (Figures 6G). For example, Kdm5b, Glis2, Smad3 and DNAjc6 were upregulated by Irx5 and Plag1 and downregulated by Smad1 (Figure 6I, upper left). H3K4me2/3 demethylase Kdm5b is a potent suppressor of AML aggressiveness [15]. Glis2 is a developmental transcription factor implicated in the control of AML cell differentiation [61]. Smad3 is a central mediator of signals from TGFβ-like proteins widely implicated in leukemia [62,63], whereas Smad1 mediates signals from BMP proteins [38]. Downregulation of Smad3 by Smad1 suggests an interesting negative crosstalk between BMP and TGFβ signaling, reminiscent of reported TGFβ mediated repression of BMP targets in various contexts [64]. Together with Smad3 upregulation by Irx5 and Plag1, this implies opposite roles of BMP and TGFβ pathways in controlling aggressiveness. Meis2, oncogenic factor in MN1-induced leukemia and AML1-ETO AML [65], and Bmx, a Tec kinase contributing to drug resistance in AML [66], were downregulated by Irx5 and Plag1 and upregulated by Smad1 (Figure 6H,I).

Smad1 overexpression downregulated central DNA methylation and chromatin remodeling factors, which were often co-regulated by Irx5 or Plag1 (Figure 6I, lower row). For example, DNA methylase Dnmt3a and histone deacetylase Hdac11 were downregulated by Smad1 and upregulated by Plag1; whereas key DNA demethylation components Tet1 and Tet2 were downregulated by Irx5 and Plag1, respectively. DNA methylation and demethylation machineries, especially DNMT3A and TET2 are strongly involved in myeloid malignancies including AML [7,67,68], consistent with the enrichment of DNA methylation and demethylation targets among DEGs associated with aggressiveness (Figure 2G) and with Irx5, Plag1 and Smad1 overexpression (Figure 6F).

Collectively, downstream effects of Smad1, Irx5, and Plag1 converged on key transcription factors (Figure 6I, black), chromatin remodelers (Figure 6I, red), and components of DNA methylation machinery (Figure 6I, blue). Aggressiveness driver Smad1 tended to downregulate repressive epigenetic factors (Polycomb proteins, histone deacetylases and demethylases, de novo DNA methylases), whereas aggressiveness suppressors Irx5 and Plag1 tended to have opposite effects. Involvement of these epigenetic repressors in the origin and maintenance of leukemia has been emerging in the literature [67], and our results suggest their involvement in the development of leukemic aggressiveness. At least one of these modifiers, histone H3K4 demethylase Kdm5b, is a direct suppressor of AML aggressiveness[15], suggesting that the broader set of Irx5, Plag1, and Smad1 targets may include new candidate regulators of leukemic aggressiveness.

DISCUSSION

Clonal evolution in blood cancers is driven by the selection of advantageous genetic and epigenetic alterations [1,5]. Genomic analyses suggest that although the origination of myeloid malignancies involves a relatively small number of mutations [69], the clonal evolution of aggressiveness is heterogeneous and can be driven by various additional genetic lesions in individual subclones [1,2,5] during unperturbed clonal evolution or as adaptation to therapy [3,4]. Disease phenotype, prognosis, and therapy response are also affected by the temporal order of these lesions [70] and progenitor stage where they appear [71], recently studied at single-cell resolution [72,73]. This heterogeneity is also apparent in single-cell gene expression [16,17]. The dynamics of chromatin landscape in clonal evolution have not been studied to the same extent, despite strong evidence of the essential role of chromatin modifiers.

Here we analyzed genome-wide dynamics of transcription and chromatin marks during the development of clonal aggressiveness and showed how these dynamics can reinforce a shared cellular program that enables clonal growth advantage. These dynamics were more clone-specific than upon initial leukemogenesis, consistent with transcriptional heterogeneity among human AML clones [16,17]. However, there was a considerable overlap between these clonal changes. The global skew towards increasing H3K4 methylation at promoters and enhancers (Figures 2J and 3H) was consistent with the reported role of H3K4me2/3 demethylase Kdm5b as a suppressor of clonal AML aggressiveness [15]. The global skew towards increasing H3K27 acetylation at enhancers, which could be uncoupled from H3K4 methylation (Figure 3H), was consistent with the role of HATs and HDACs in AML.

Unexpectedly, most of the involved promoters and enhancers were already affected at the early leukemic stage of the same clone (Figures 2H, 3F, S3L, S4H). More surprisingly, rather than developing further, these early changes were most often reversed at the aggressive stage (Figures 2I, 3G, S3M, S4I). This reversal is consistent with the reported changes in the roles of some central leukemic regulators at later stages of AML; Polycomb component Ezh2 is a strong tumor suppressor during AML induction and is later switched to an oncogenic role during AML maintenance [14], and Igf1r is a major oncogene during AML induction but is not required during later clonal growth [52]. The biological role of this reversal is an important question. As one possible explanation, the initial leukemogenic lesion (MLL rearrangement) causes perturbations across a wide variety of direct and indirect genomic targets (Figure 1D,L), some of which (activation of Hoxa9, Meis1, etc) cause oncogenic transformation, while others may be non-essential and even maladaptive for later clonal fitness and growth. In this case, scaling back maladaptive initial effects (Figure 2C, 3C, 4D,F) while keeping strong initial activation of leukemogenic drivers (Figure 1C)

may provide a growth advantage. This reversal may be achieved through the regulation of promoters and enhancers by transcription factors and chromatin regulators.

Focusing on consistent changes of expression and chromatin marks in both clones in vivo and ex vivo revealed the core gene set (Figures 4A,B), which strongly followed this reversal trend, often paralleled by nearby enhancers (Figures 4G,H). We selected three of these genes for experimental validation and confirmed their causal roles as leukemic cell growth suppressors (Irx5 and Plag1) and activator (Smad1). These roles are consistent with public data in human hematopoiesis and AML. Irx5 is a curious example of a strong MLL-AF9 target [49] that was released from Polycomb repression and dramatically activated at the early leukemic stage, like known major leukemogenic drivers (Figure 4D). However, unlike these drivers, at the aggressive stage Irx5 reversed this activation by increased Polycomb repression (Figure 4D). Plag1 is an oncogene derepressed at the induction of AML [14,50], but it's surprising opposite role in suppressing clonal aggressiveness has not been previously reported. SMAD1 has not been reported as a major leukemic regulator, although it is a central effector of the BMP pathway implicated in leukemia [38,39]. Smad1 was the only Smad family member with this behavior, which positions BMP pathway as a possible therapeutic target distinct from the related TGFβ pathway.

Downstream transcriptional effects of these three genes upon their overexpression converge on a network of transcription factors, chromatin modifiers, and components of DNA methylation machinery, many strongly implicated in leukemia (Figure 6I). The effects on Smad3, a key effector of TGFβ pathway (Figure 6I), may suggest that Smad3-mediated TGFβ signaling is inhibited and replaced by Smad1-mediated BMP signaling in aggressive subclones. This inhibition is in line with

aggressivenss-associated regulation of other TGFβ related genes (Peg10, Matn2, Ptpn3, Figure 4B).

Coordinated downstream regulation also affects major epigenetic factors: H3K4me2/3 demethylase Kdm5b, Polycomb component Bcorl1 [58,59], as well as DNA methylase Dnmt3a [7] and DNA demethylation component Tet2 [8], highlighting the role of repressive Polycomb, H3K4 demethylation, and DNA methylation machineries. Modulation of Polycomb repression was a major mechanism of promoter regulation at both early and aggressive leukemic stages, for example at *Smad1*, *Irx5*, and *Plag1* (Figure 4C-F). The reported role of Kdm5b as aggressiveness suppressor in leukemia [15] was consistent with its transcriptional regulation by Smad1, Irx5, and Plag1 (Figure 6I) and the global skew towards increased promoter (Figures 2J) and enhancer H3K4 methylation (Figure 3H) at the aggressive stage. DNA methylation and demethylation components with known strong AML involvement[7,8] were regulated by Smad1 and Plag1 in opposite directions (Figure 6I). This collective involvement of epigenetic repressors is consistent with their known functional crosstalk. In addition to antagonism between Polycomb and H3K4 methylation [23], as well as direct Polycomb repression of Kdm5b [15], there is growing evidence of direct Polycomb-DNMT3A interactions [74] contributing to leukemia [75].

Taken together, our results suggest that development of aggressiveness is a clone-specific process often mediated through gradual adjustment of chromatin state and gene expression, as opposed to on/off switch behavior typical for major leukemogenic drivers. This adjustment often involves a surprising reversal of prior expression and chromatin state changes at the early leukemic stage. We identified a set of core genes with aggressiveness-associated changes consistent between clones and between in vivo and ex vivo conditions, and successfully validated three genes as causal

regulators of leukemic cell growth with convergent downstream transcriptional effects, suggesting new candidate pathways in regulating leukemic aggressiveness.

LIMITATIONS OF THE STUDY

In this study we used a well-established mouse model of AML driven by the MLL-AF9 fusion [18]. Although it was shown to faithfully recapitulate many aspects of human AML, a mouse model may limit direct applicability of our results to human disease. Focusing on one specific AML subtype driven by MLL fusions also limits the scope of our findings, although our analyses of public data from AML patient cohorts provide a wider context of behavior of the three aggressiveness regulators among various other AML subtypes. Although BMP pathway inhibitor LDN-212854 suppressed the growth of mouse leukemic cell lines, this inhibitor exhibited toxicity in mice. In assessing the associations between patient survival and the expression of the aggressiveness regulator genes, we used public data across all AML patients, as we did not have access to SMAD1, IRX5, and PLAG1 expression data linked to the survival data among the more focused cohort of patients with MLLr AML.

ACKNOWLEDGEMENTS

R.I.S. was supported by NIH NIDDK P30 DK040561. DBS was supported by grants from the St. Baldrick's Foundation and the American Society of Hematology.

DECLARATION OF INTERESTS

DBS is a co-founder and holds equity in Clear Creek Bio.

FIGURE LEGENDS

Figure 1. Chromatin and gene expression changes between normal and early leukemic progenitors were consistent between independent clones and mostly maintained through the later aggressive stage.

A. A mix of leukemic clones individually labeled with different flurorescent proteins was transplanted in a primary mouse recipient, followed by clonal evolution for 120 days and collection of aggressive subclones, which maintained their aggressiveness upon secondary transplantation. The early and aggressive stages of two leukemic clones were profiled by RNA-seq in vivo and ex vivo, and by ChIP-seq of histone marks ex vivo, and compared to normal progenitors. **B.** Promoter chromatin state of a major leukemogenic driver Meis1 was dramatically activated in leukemic cells compared to normal but showed no strong difference between two stages of aggressiveness. ChIP-seq genomic tracks of H3K27me3 (red), H3K4me3 (blue), and H3K27ac (green) in normal progenitors (top) compared to two independent leukemic clones 1 and 2 at early and aggressive stages. **C.** Known drivers of MLLr leukemia were activated at the early stage but did not show further changes at the aggressive stage. Promoter chromatin state progression for Meis1 (tracks in **B**), HoxA9, and Six1 (tracks in Figure S2) in the space of H3K27me3 (x axis) vs H3K4me3 density (y axis) at TSS-proximal region. Normal progenitors and early and aggressive stages of two leukemic clones (1 and 2) are represented as grey, blue, and red points, respectively. Gene expression levels (RNA-seq RPKM) are shown as barplots. Early loss of repressive H3K27me3 mark accompanied by strong gain of active H3K4me3 mark (arrows) and upregulation of expression were later maintained at the aggressive stage. **D.** Heatmap of early changes (log2 fold change) of promoter chromatin marks across all promoters with a substantive absolute level and > 2-fold change of at least one mark, juxtaposed with the changes of gene expression in vivo (log2 fold change, right). Changes

were strongly consistent in two independent clones (two columns for each mark and expression). **E.** Venn diagrams of a strong overlap between the early stages of two independent clones (Early 1, Early 2) among promoters with differential gene expression in vivo (purple) and chromatin mark density (green, blue, and red) compared to normal progenitors. **F.** Functional category enrichment among genes differentially expressed between normal and early leukemic progenitors in vivo consistently in both clones. Bars colored by category types represent adjusted P-value of enrichment according to EnrichR. **G.** In both clones, early-stage changes were skewed towards the increase of active H3K27ac and H3K4me3 promoter marks and gene expression and decrease of repressive mark H3K27me3. Barplots of promoter numbers with increase (red) and decrease (blue) of each individual mark and gene expression at the early stage in each leukemic clone (Early 1, Early 2). **H.** Most of the early changes of promoter chromatin marks and expression were later maintained at the same level at the aggressive stage. Scatterplots of chromatin mark changes (log2 fold change) at all promoters between normal cells and the early leukemic stage (y axis) compared to the changes between normal cells and the aggressive leukemic stage (x axis). Individual promoters are represented as points, color indicates point density. **I.** Genome-wide trends among the early leukemic changes of promoter chromatin states. All promoters across the genome are represented as points in the space of H3K27me3 (x axis) vs H3K4me3 density (y axis) at TSS-proximal region. Each point is colored by gene expression in normal progenitors, from blue (silent) to red (active). Upper left: active promoters enriched in H3K4me3 and depleted in H3K27me3. Middle right: bivalent promoters with high H3K27me3 and moderate H3K4me3. Lower left: silent promoters with both marks depleted. Arrows with corresponding promoter numbers indicate major directions of H3K4me3/ H3K27me3 changes. **J.** Example of ChIP-seq tracks at two enhancers that changed chromatin state at the early leukemic stage. H3K27ac (green) and H3K4me1 (dark green) densities in normal progenitors (top) compared to two independent leukemic clones 1 and 2 at the

early and aggressive stage. **K.** Chromatin state progression at enhancers proximal to Des (shown in **J**), Lmo1, and Pitx2 genes in the space of H3K4me1 (x axis) vs H3K27ac density (y axis). Points represent normal progenitors (grey) and the early (blue) and aggressive (red) stages of two leukemic clones (1 and 2). **L.** Heatmap of the early leukemic changes (log2 fold change) of H3K4me1 and H3K27ac densities across all enhancers with a substantive absolute level and > 2-fold change of at least one mark, juxtaposed with the changes of proximal gene expression in vivo (log2 fold change, right). Changes were largely consistent between marks and between two independent clones (two columns for each mark and expression). **M.** Venn diagrams of a strong overlap between between two clones (Early 1, Early 2) among enhancers with chromatin mark changes between normal progenitors and the early leukemic stage. **N.** Most of the early changes of enhancer chromatin marks were later maintained at the aggressive stage. Genome-wide scatterplots of chromatin mark changes (log2 fold change) at all enhancers between normal cells and the early leukemic stage (y axis) compared to the changes between normal cells and the aggressive leukemic stage (x axis). Individual enhancers are represented as points; color indicates point density. **O.** Genome-wide trends among the early leukemic changes of enhancer chromatin states. All enhancers across the genome are represented as points in the space of H3K4me1 (x axis) vs H3K27ac density (y axis). Each point is colored by proximal gene expression in normal progenitors, from blue (silent) to red (active). Arrows with corresponding enhancer numbers indicate major directions of H3K4me1/ H3K27ac changes.

Figure 2. Changes of promoter chromatin state and expression between the early and aggressive leukemic stages were more clone-specific, gradual, and often reversed the early leukemic changes.

A,B. Examples of ChIP-seq genomic tracks showing promoter chromatin mark and expression changes between two stages of aggressiveness. H3K27me3 (red), H3K4me3 (blue), and H3K27ac (green) densities in normal progenitors (top) compared to two independent leukemic clones 1 and 2 at early and aggressive stages. Compared to normal progenitors, Fhdc promoter was activated (**A**) and Fyb promoter was repressed (**B**) to a different degree between the early and aggressive stage of the same clone. **C.** Promoter chromatin state progression for Fhdc and Fyb promoters (tracks shown in **A, B**) in the space of H3K27me3 (x axis) vs H3K4me3 density (y axis) at TSS-proximal region. Points represent normal progenitors (grey) and early (blue) and aggressive stages (red) of two leukemic clones (1 and 2). Strong opposite shifts of H3K27me3 and H3K4me3 at the early stage of both clones (blue arrow) were later partially reversed at the aggressive stage (red arrow), concomitant with changes of gene expression (barplots of RNA-seq RPKM). **D.** Heatmap of changes (log2 fold change) of promoter chromatin marks between the early and aggressive stages across all promoters with a substantive absolute level and > 2-fold change of at least one mark, juxtaposed with the changes of gene expression in vivo (log2 fold change, right). Changes were only partially consistent between two independent clones (two columns for each mark and expression). **E.** Principal component analysis (PCA) plot of gene expression in normal progenitors (grey) compared to early (blue) and aggressive stage (red) of two leukemic clones (1 and 2). **F.** Venn diagrams of moderate overlap between two independent clones (Aggressive 1, Aggressive 2) among promoters with changes of gene expression in vivo (purple) and chromatin marks (green, blue, and red) at the aggressive stage. **G.** Functional category enrichment among genes differentially expressed between the early and aggressive stages in vivo consistently in both clones. Bars colored by category types represent adjusted P-value of enrichment according to EnrichR. **H.** Most promoters affected at the aggressive stage underwent prior changes at the early leukemic stage. Venn diagrams of promoters with changes of expression and individual chromatin marks at

the aggressive and early stages of the same clone. **I.** Among promoters that underwent consequent changes at both leukemic stages, the majority reversed their initial early changes. Large arrows (Early 1, Early 2): numbers of promoters with increase (red) and decrease (blue) of expression or a chromatin mark at the early leukemic stage of a clone (1 and 2). Adjacent smaller arrows (Aggressive 1, Aggressive 2): numbers of these promoters with the later increase (red) or decrease (blue) of expression or chromatin mark at the aggressive stage. **J.** Genome-wide trends among changes of promoter chromatin states at the aggressive stage (representative example of one clone). All promoters across the genome are shown as points in the space of TSS-proximal H3K27me3 (x axis) vs H3K4me3 densities (y axis) at the early leukemic stage, colored by the level of gene expression from blue (silent) to red (active). Arrows with corresponding promoter numbers indicate major directions of H3K4me3/ H3K27me3 changes at the aggressive stage. Yellow, preferential skews that were consistent between clones.

Figure 3: Enhancer chromatin remodeling at the aggressive stage was more clone-specific, skewed towards activation, and often reversed early leukemic changes.

A,B. Examples of ChIP-seq genomic tracks showing enhancer chromatin mark changes between two stages of aggressiveness. H3K27ac (green) and H3K4me1 (dark green) densities in normal progenitors (top) compared to two independent leukemic clones 1 and 2 at the early and aggressive leukemic stages. Chromatin state of an intronic enhancer in Net1 gene became more active (**A**) and chromatin state of an enhancer proximal to gene Zfp516 became less active at aggressive compared to early stage in both clones (**B**). **C.** Chromatin state progression in the space of H3K27ac vs H3K4me1 density at enhancers shown in **A, B.** Points represent normal progenitors (grey) and the early (blue) and aggressive stages (red) of two leukemic clones (1 and 2). Changes between the early and aggressive stages (red arrows) were accompanied by proximal gene expression

changes (barplots of RNA-seq RPKM). **D.** Heatmap of H3K27ac and H3K4me1 density changes (log2 fold change) at the aggressive stage across all enhancers with a substantive absolute level and > 2-fold change of at least one mark, juxtaposed with the changes of gene expression in vivo (log2 fold change, right). Changes were only partially consistent between two independent clones (two columns for each mark). **E.** Venn diagrams of moderate overlap between two independent clones (Aggressive 1, Aggressive 2) among enhancers with changes of H3K27ac (green) and H3K4me1 (dark green) between the early and aggressive leukemic stages. **F.** Most enhancers affected at the aggressive stage underwent prior changes at the early stage. Venn diagrams of enhancers with changes of H3K27ac and H3K4me1 at the aggressive and early stages of the same clone. **G.** Among enhancers that underwent consequent changes at both leukemic stages, the majority reversed their initial early changes. Large arrows (Early 1): numbers of enhancers with the early increase (red) and decrease (blue) of H3K27ac in clone 1. Adjacent smaller arrows (Aggressive 1): numbers of these enhancers with the later increase (red) or decrease (blue) of H3K27ac at the aggressive stage. Data for clone 2 in Figure S4I. **H.** Genome-wide trends among changes of enhancer chromatin states at the aggressive stage (representative example of one clone). All enhancers across the genome are shown as points in the space of H3K4me1 (x axis) vs H3K27ac density (y axis) at the early leukemic stage, colored by the level of proximal gene expression from blue (silent) to red (active). Arrows with corresponding enhancer numbers indicate major directions of H3K4me1/ H3K27ac changes between the early and aggressive stages. Yellow, preferential skew towards H3K27ac increase reversed the opposite early trend (Figure 1O). **I.** Enrichment of transcription factor binding motifs associated with enhancer mark changes at the aggressive stage. MEME enrichment E-values for transcription factor motifs (rows) shown for enhancers changing the level of a given chromatin mark in a given clone (columns). **J.** Enhancer H3K27ac level is often quantitatively correlated with the expression of the proximal gene.

Correlation scatterplots of enhancer H3K27ac density vs proximal gene expression across normal progenitors (grey), early (blue) and aggressive leukemic stages (red) for two enhancers shown in **A-C**. Pearson correlation coefficient and linear regression P-value are indicated. **K.** Enhancers increasing H3K27ac at the aggressive stage show preferential positive correlation of H3K27ac level with proximal gene expression. Histogram of all Pearson correlation coefficients between enhancer H3K27ac and gene expression (calculated as in **J**) is strongly skewed towards higher R and includes a distinct enhancer subset with strong correlation (R > 0.7, dotted line). **L.** Functional category enrichment among genes proximal to the enhancer subset shown in **K**. Bars colored by category types represent adjusted P-value of enrichment according to EnrichR.

Figure 4. Core genes with consistent aggressiveness-associated differences of promoter chromatin state ex vivo and expression in vivo in both independent clones.

A. Filtering genes by the consistency of aggressiveness-associated changes of gene expression in vivo (yellow) vs active H3K27ac and H3K4me3 (blue) and repressive H3K27me3 (red) promoter marks ex vivo in both clones. Numbers of promoters with expression or chromatin mark increase and decrease are indicated in red and blue, respectively. A core set of 28 candidate genes had fully consistent behavior across all comparisons. **B.** Heatmap of promoter H3K27me3, H3K4me3, H3K27ac and expression changes (fold change in log2 scale) for the core gene set between the early and aggressive stage of two clones. **C.** Examples of genomic ChIP-seq tracks at Irx5 (left) and its proximal enhancer (right) where the magnitude of the early leukemic activation was later adjusted at the aggressive stage. **D.** Examples of promoter chromatin state progression in the space of H3K27me3 (x axis) vs H3K4me3 (y axis) for core genes Irx5 (tracks in **C**) and Plag1 (tracks in Figure S5B). Points represent normal progenitors (grey) and early (blue) and aggressive stages (red) of two leukemic clones (1 and 2). H3K27me3 loss and H3K4me3 gain at the early leukemic

stage of both clones (left plots, blue arrows) were later partially reversed at the aggressive stage (left plots, red arrows), consistent with in vivo expression changes (right barplots). These changes were paralleled by H3K27ac and H3K4me1 at a proximal enhancer (middle plots). **E.** Examples of genomic ChIP-seq tracks at Smad1 (left) and its proximal enhancer (right) where the magnitude of the early leukemic repression was later adjusted at the aggressive stage. **F.** Examples of promoter chromatin state progression in the space of H3K27me3 vs H3K4me3 for core genes Smad1 (tracks shown in **E**) and Rxra (tracks in Figure S5C). H3K27me3 gain and H3K4me3 loss at the early leukemic stage of both clones (left plots, blue arrows) were later partially reversed at the aggressive stage (left plots, red arrows), consistent with in vivo expression changes (right barplots). These changes were paralleled by H3K27ac and H3K4me1 at a proximal enhancer (middle plots). **G.** Virtually all core aggressiveness-associated genes underwent prior changes at the early leukemic stage. Venn diagrams of promoters with aggressiveness-associated (Aggressive) and early leukemic changes in the same clone (Early) for expression and individual chromatin marks (representative example of one clone, additional clone in Figure S5D). **I.** Among the core genes that underwent consequent changes at both leukemic stages, the majority reversed their initial early changes (representative example of one clone, additional clone in Figure S5E). Large arrows (Early 1): numbers of promoters with the early increase (red) and decrease (blue) of expression or a chromatin mark in clones 1 and 2. Adjacent smaller arrows (Aggressive 1): numbers of these promoters with later increase (red) or decrease (blue) of expression or chromatin mark at the aggressive stage.

Figure 5. Effects of overexpressing selected core genes validate their causal roles

A. Smad1 and Kras G12V mutant (used as a control) were overexpressed in the early stage subclone, whereas Irx5 and Plag1 were overexpressed in the aggressive stage subclone of the

same leukemic clone. Barplots of RNA-seq gene expression values (RPKM) in transduced compared to control untransduced cells (n=3 biological replicates). **B.** Overexpression of Smad1 increased, whereas overexpression of Irx5 and Plag1 decreased cell growth. Ex vivo cell growth curves and the corresponding doubling times for transduced cells compared to untransduced controls. Data are represented as mean +/- SEM. **C.** Representative images of Wright-Giemsa–stained cells transduced with each gene, compared to control. Scale bar, 1 micron. **D.** Colony forming efficiency by transduced clones did not show strong changes compared to control. Barplot of colony numbers in methylcellulose (mean and SD, n=2) per 1500 cells. **E.** Examples of individual colonies formed by the transduced cells compared to the control early and aggressive subclones. **F.** Flow cytometry analysis of c-Kit, Gr1, CD123, and CD11b expression in each transduced subclone compared to control suggest no strong changes of myeloid hematopoietic lineage. **G.** Median c-Kit fluroscence intensity in the transduced cells compared to the control early and aggressive subclones. **H.** Fractions of cell cycles phases (G1, S, G2/M) for the transduced cells compared to the control early and aggressive subclones. **I.** Annexin V apoptosis assay. Left, gating strategy (example). Right, barplot of fractions of apoptotic (Annexin+ / DAPI-) and dead cells (DAPI+). **J.** Dose dependency curve of a ALK2/BMP pathway inhibitor LDN212854 in the early (blue) and aggressive (red) leukemic subclones compared to normal non-leukemic mouse progenitors (gray) ex vivo.

Figure 6. The roles of Smad1, Irx5, and Plag1 are supported by AML patient data and convergent downstream effects on a common regulatory network.

A. High IRX5 expression is significantly associated with longer overall survival in AML patients. Analysis of TCGA AML patient cohort implemented in BloodSpot. Kaplan-Meier curves for AML patients with IRX5 expression above (red) and below median (green).

B. Violin plots showing the distributions of SMAD1, IRX5, and PLAG1 expression (log2 scale) within various AML subtypes compared to healthy control group (pink, right). SMAD1 is downregulated in MLL-rearranged AMLs. IRX5 is upregulated across major AML subtypes. PLAG1 expression in MLL-rearranged AMLs is not significantly different from normal control and modestly downregulated in some other AML subtypes. **C.** Analysis of previously published single-cell RNA-seq data in granulocyte/macrophage progenitors (GMPs) from AML patients [16] confirms lower expression of SMAD1 and higher expression of IRX5 and PLAG1 in human leukemic progenitors. These differences are smaller but similar in scale to the expression differences for a major leukemic driver HOXA9. **D.** SMAD1, IRX5, and PLAG1 expression levels in public data from normal human myeloid lineage (GEO GSE42519) and various AML types (GEO GSE13159), analyzed in BloodSpot. SMAD1 is highly expressed whereas IRX5 and PLAG1 are silent in normal human GMPs. SMAD1 is downregulated whereas IRX5 is upregulated specifically in MLLr AML t(15;17). PLAG1 expression is low across AML types. **E.** Genome-wide transcriptional changes caused by Smad1 overexpression in mouse leukemic progenitors are largely opposite to the changes caused by Irx5 and Plag1 overexpression. Heatmap of RNA-seq expression changes compared to control (log2 fold change) among genes differentially expressed (> 2 fold change, FDR < 0.05) in any of the three transduction experiments. **F.** Overlap of functional categories enriched among genes up- and downregulated (bars to the right and left of dotted line, respectively) by Irx5, Plag1, and Smad1 overexpression. Bars colored by category types represent 10log10 of adjusted P-value of enrichment according to EnrichR. **G.** Overlaps between downstream transcriptional effects of the three overexpressed genes. Venn diagrams of the genes downregulated by Plag1 and Irx5 and upregulated by Smad1 (top), and of the genes upregulated by Plag1 and Irx5 and downregulated by Smad1 (top). Hypergeometric P-values for pairwise overlaps are indicated. **H.** Heatmap of RNA-seq expression changes compared to control (log2 fold change) for selected downstream targets

consistently affected by Smad1, Irx5, and Plag1 overexpression. **I.** Smad1, Irx5, and Plag1 effects suggest a common downstream regulatory network (schematic).

STAR METHODS

Experimental model and study participant details

Murine models and cell lines

Experiments were approved by the Institutional Animal Care and Use Committee (IACUC) of the Massachusetts General Hospital. C57BL/6J, B6.SJL-Ptprca Pepcb/BoyJ (CD45.1) were purchased from Jackson Laboratories. All MLL-AF9 leukemic cell lines were obtained as previously described [76] and maintained in RPMI1640 (10% FBS), penicillin/streptomycin, 6 ng/ml rmIL-3, and approximately 100 ng/ml SCF. Briefly, a MLL-AF9 CD45.1 parental line was established by sorting, using a FACS AriaII (BD Biosciences), granulocyte-macrophage progenitors (GMP; c-Kit^{high}Sca-1^{-} Gr-1^{low}CD16/32^{+}CD34^{+}) from a male CD45.1 donor. Retrovirally transfection with a MSCV-MLL/AF9-IRES-NeoR construct in sorted progenitor cells was performed a day after incubation in RPMI1640 (Lonza) transduction medium containing 10% (FBS; Gibco), 100 I.U./ml penicillin, 100 mg/ml streptomycin (Gibco), 10 ng/ml recombinant mouse SCF (rmSCF), 6 ng/ml recombinant mouse interleukin 3 (rmIL-3), 5 ng/ml rmIL-6 (all from Peprotech). Progenitors were transferred to RetroNectin®-coated (Lonza) 6-well plates in a volume of 1 ml, combined with 1 ml of fresh retroviral supernatant packaged in 293FT cells (Invitrogen) with pCL-Eco (Addgene 12371) and 8 µg/ml final concentration of polybrene, then spinoculating (1,000g, 90 min, 22°). Immediately following the transduction, 4 ml of fresh transduction medium was added to each well to dilute the polybrene and 24 hours post-transduction, cells were washed by centrifugation (500g, 5 min, 4°C) then resuspended in fresh transduction medium. 48 hours post-transduction, neomycin resistant lines were selected using 50 µg/ml neomycin (Gibco).

Method details

Clonal fluorescent labeling

To generate MLL-AF9 clones expressing fluorescent proteins (FP), single MLL-AF9 CD45.1 clones were sorted using a FACS Aria II (BD Biosciences) into 96-well plates. A single clone was expanded and transduced with lentiviral constructs EF1a-FP-SV40-PuroR, generated by Gateway cloning of FP Entry plasmids into the pLEX_307 Destination construct (a gift from David Root, Addgene plasmid # 41392). From each FP transduction, single subclones were expanded in vitro and those that stably expressed FPs were preserved.

Syngeneic leukemia experiments

All leukemia transplantations were performed by injecting cells intravenously (tail vein) in a volume of 300 ul of phosphate-buffered saline (PBS) in recipient C57Bl/6J male mice (age 8-10 weeks) that were sublethally irradiated (4.5Gy) the day prior using a Cesium-137 source. Blood was collected through tail vein sampling and complete blood counts were done on a Heska Element HT5 analyzer. Bone marrow aspiration was done under isoflurane anaesthesia using a 25G needle attached to a 1 ml syringe rinsed with PBS, gently inserted into the femoral cavity through the articular surface of the knee; approximately 10 µl of bone marrow was gently aspirated in the syringe and immediately resuspended in 300 µl of PBS on ice. Hematopoietic cell isolation was done as follows: after euthanasia by asphyxiation with CO_2, vertebrae and the long bones of the arms and legs were dissected and crushed into PBS containing 2% FBS (FACS buffer). The bone marrow mononuclear cells were isolated over a Ficoll-Paque PLUS density gradient and counted using trypan blue and the Cellometer instrument.

Overexpression of gene candidates

Leukemic subclones were cultured in RPMI 1640 medium supplemented with 10% fetal bovine serum, 1% L-glutamine, 1% penicillin/streptomycin, 25 ng/mL SCF, and 5 ng/mL IL-3. ORFs of

interest were overexpressed using second-generation lentiviral system that consisted of pCMV-VSV-G (Weinberg lab) envelope plasmid and PsPAX2 (Trono lab) packaging plasmid acquired from Addgene. HEK293t cells were transfected with plasmid DNA at a ratio of 5:4:1 transfer plasmid:envelope plasmid:packaging plasmid. Transfection efficiency was aided by the addition of Promega's Fugene6 Reagent at a ratio of 3:1 to plasmid DNA. HEK293t cells were cultured in DMEM, high glucose, pyruvate supplemented with 10% fetal bovine serum and 1% penicillin/streptomycin. Lentiviral titer was assessed by FACS. Mouse leukemic progenitors were transduced by exposing them to viral particles and room temperature centrifugation at 1000g for 1 hr in 8uG/mL polybrene (Millipore Sigma). Spinfection plates were pre-coated using 500 uL of PBS with 10 uG/mL of purified human plasma fibronectin (Sigma-Aldrich) and incubated at 37°C several hours prior to transduction. Single cell FACS sorting was performed 48 hours after transduction to isolate individual GFP-positive clones. Overexpression of the gene of interest in selected clones was confirmed by RT-qPCR and RNA-seq. RNA was extracted using TRIzol LS Reagent, followed by cDNA synthesis using SuperScript First-Strand Synthesis System for RT-PCR (Invitrogen).

Cell growth quantitation

Cell growth was quantitated using CellTrace Far Red Cell Proliferation Kit (Invitrogen), Initially, on day 1, cell lines were standardized to a density of 1,000,000 cells/mL in 1mL of PBS, labeled with CellTrace™ Far Red dye at a 1 μM concentration, and subsequently centrifuged at 500g for 5 minutes and resuspended in fresh media. The labeled cells were then cultured in 6-well plates containing 5 mL of RPMI 1640 media supplemented with 10% Fetal Bovine Serum. Starting on day 2, daily sampling was conducted by aspirating a fraction of the culture, centrifuging at 500g for 5 minutes, and resuspending the cell pellet in 400 μL FACS Buffer containing 0.8% formaldehyde for overnight fixation. The following day, formaldehyde fixation was neutralized with the addition of 100 μL FBS. These fixed samples were stored at 4°C until the final timepoint. Flow cytometric analysis

was performed on a BD FACS Melody system, where the mean fluorescence intensity of each sample was measured at every timepoint. The doubling time was inferred by calculating the time interval required for the fluorescence intensity to halve, reflecting cell proliferation rates.

Cell sorting to assess hematopoietic lineage

Cellular suspensions were prepared for flow cytometric analysis by harvesting 1 million cells and resuspending them in 100 µL of FACS Buffer, consisting of 2% fetal bovine serum, 1 mM EDTA, and phosphate-buffered saline. The cell suspensions were then labeled with lineage related antibodies: PE/Dazzle™ 594 anti-mouse/human CD11b (Biolegend 101256), APC anti-mouse Ly-6G/Ly-6C (Gr-1) (Biolegend 108412), PE anti-mouse CD123 (Biolegend 106005), and PE/Cyanine7 anti-mouse CD117 (c-kit) (Biolegend 135112), at the appropriate concentrations for the volume and cell count (1uL in 1 million cells), followed by incubation at room temperature for 30 minutes in the dark. Post-incubation, cells were centrifuged at 500g for 5 minutes, washed twice with FACS Buffer, and finally resuspended in 400 µL of the same buffer. The cell suspensions were then strained through a 70 µm mesh into FACS tubes to ensure a single-cell suspension. Single-color controls were established using OneComp eBeads™ (Thermofisher 01-1111-41). Analysis was performed in FlowJo, with doublet discrimination and fluorescent compensation.

Cell Cycle Assay

Cells were grown out for two days and resuspended at 10 million cells/mL in 1X Dulbecco's Phosphate Buffered Saline (DPBS) (Life Technologies Limited, Paisley, PA, USA). 3 million cells were then transferred to a FACS tube and chilled on ice for 5 minutes. Ice cold ethanol (Sigma-Aldrich, Burlington, VT, USA) was added while samples were vortexed. Tubes were then stored at -20˚C overnight. 3mL of 1X DPBS was added to each tube and tubes were spun down at 500g for 5 minutes. Cells were then resuspended in 300µl of staining buffer (0.4 mg/mL RNAse A (Thermofisher, Waltham, MA, USA), 10 uG/mL propidium iodide (Life Technologies Corporation,

Eugene, OR, USA), 0.1% Triton X-100 (Sigma-Aldrich, St. Louis, MO, USA) in PBS) and filtered through a 40µm Corning Cell Strainer (Corning Incorporated, Durham, NC, USA) into FACS tubes. Samples were then incubated at 37˚C for 15 minutes and flowed on a Becton-Dickinson (BD) FACSCelesta instrument to collect 10,000 events per sample. Flow cytometry data was analyzed using FlowJo v10.10 (BD Biosciences, Ashland, OR, USA).

Annexin V Apoptosis Assay

A modified protocol provided by Biotium was used to prepare samples. 5X Annexin V Binding Buffer (Biotium, Fremont, CA, USA) was first diluted with Ambion nuclease-free water (Invitrogen, Austin, TX, USA) at a 1:5 ratio. Cultured cells were washed with 1X Dulbecco's Phosphate Buffered Saline (DPBS) (Life Technologies Limited, Paisley, PA, USA) once and resuspended at 3,000,000 cells/mL in diluted binding buffer. Annexin V Conjugate CF 633 (Biotium, Fremont, CA) was added to 100µl of each cell type for a final concentration of 1µg/mL. Cells were incubated at room temperature for 30 minutes in the dark and then washed with 1X DPBS once before staining with 4',6-diamidino-2-phenylindole, dihydrochloride (DAPI) (Invitrogen, Austin, TX, USA). 1X Binding Buffer was then added to each tube and tubes were flowed on a Becton-Dickinson (BD) FACSCelesta instrument to collect 10,000 events per cell line. Flow cytometry data was analyzed using FlowJo v10.10 (BD Biosciences, Ashland, OR, USA).

Methylcellulose colony forming assay

A modified protocol from StemCell Technologies was used to culture cell lines in methylcellulose. MethoCult GF M3434 (StemCell Technologies, Canada) was thawed overnight at 4˚C. Cells were counted using Acridine Orange/Propidium Iodide Stain (Aligned Genetics, Inc., Annandale, VA, USA) and diluted to 50,000 cells/mL. Cells were counted again and ~1500 cells were added to each MethoCult GF M3434 tube. Tubes were shaken vigorously and allowed to settle for 5 minutes. A 3mL syringe and 18 gauge 1-1/2 inch needle were used to plate 1.1mL of MethoCult in

35mm plates in duplicate. Each 35mm plate was placed inside a 10cm plate along with another 35mm plate filled with sterile water. All plates were incubated at 37˚C, 5% CO_2 and counted after eight days. Mean and standard deviation based on biological duplicates were calculated for each cell type.

Assaying effects of BMP inhibitor on cell growth ex vivo

ER-Hoxb8 overexpressing progenitors used as normal control were cultured in RPMI1640 (10% FBS), 1% penicillin/streptomycin, 1% L-glutamine, 100 ng/ml SCF and 0.5 uM β-estradiol. Early and aggressive leukemic subclones as well as normal ER-Hoxb8 overexpressing progenitors were grown out, resuspended at 50,000 cells/mL in their respective media, and plated in 96-well plates at 100µl of cells per well. Cells were then treated with 10µM to 0.005µM concentrations of inhibitor LDN-212854 (Selleck Chem, Houston, TX, USA) using the D300e Digital Dispenser (Tecan Trading AG, Switzerland). Plates were then incubated at 37˚C for 3 days, after which 100µl of diluted CellTiter- Glo 2.0 Cell Viability Assay (Promega, Madison, WI, USA) (1:1 in 1X Dulbecco's Phosphate Buffered Saline (DPBS) (Life Technologies Limited, Paisley, PA, USA) was applied to each well and mixed thoroughly. Plates were then read using a BioTek Synergy HTX instrument (BioSPX, Netherlands) for fluorescence and then analyzed on Prism 10.0 for IC50 (GraphPad, Boston, MA, USA).

RNA library preparation and sequencing (RNA-seq)

Total RNA was isolated from three biological replicates of each cell type using TRIzol (Invitrogen) and DNase treated. Sequencing libraries were prepared using polyA-selection followed by NEBNext Ultra Directional RNA library preparation protocol (New England Biolabs). Sequencing was performed on Illumina HiSeq 2500 instrument, resulting in approximately 30 million 50 bp reads per sample.

Chromatin immunoprecipitation library preparation and sequencing (ChIP-seq)

Cells were crosslinked for 10 minutes in 1% formaldehyde at room temperature and quenched with 125mM Glycine. ChIP was performed as previously described [77]. Antibodies used: H3K4me1 (Abcam ab8895), H3K4me3 (Millipore, 04-745), H3K27me3 (Cell Signaling Technology, C36B11), H3K27ac (Abcam ab4729). Samples were further processed for high throughput sequencing. Sequencing was performed on Illumina HiSeq 2500 instrument resulting in approximately 30 million paired-end 50 bp reads per sample.

Quantification and statistical analysis

RNA-seq data analyses

Sequencing reads were mapped to the mouse transcriptome (mm9 EMSEMBL annotation) using STAR [78]. Gene expression counts were calculated using HTSeq v.0.6.0 [79]. Calculation of expression values and differential expression analysis were performed using EgdeR package [80] after normalizing read counts and including only genes with count per million reads (CPM) > 1 for one or more samples. Differentially expressed genes were defined based on the criteria of > 2 fold change of expression and FDR < 0.05. Analysis of gene set enrichment was performed using Enrichr [22].

ChIP-seq data analyses

Reads were aligned against the mm9 reference genome using BWA [81]. Alignments were filtered for uniquely mapped reads and alignment duplicates were removed. Input-normalized and CPM normalized coverage tracks were generated using the bamcompare function of deepTools [82]. Enrichment over TSS-proximal regions (TSS ± 3 Kb) was calculated as the ratio of ChIP and input read counts scaled by library size. Reads of publicly available MLL-AF9 ChIP-seq (GEO accession number GSE29130) were aligned as described previously, and peaks were identified using Homer

with the “factor” option. Strong targets genes of MLL-AF9 were identified by filtering the peak list using a peak enrichment cutoff >=13. Putative enhancer elements were identified using H3K27ac and H3K4me1 ChIP-Seq peaks. In brief, we analyzed tag counts in sliding 1 Kb windows with the step of 200 bp and estimated statistical significance of enrichment of ChIP vs input using negative binomial distribution with the parameter of mean based on input tag count and the size parameter (s) selected based on manual inspection of peak calls. Regions of significant enrichment were generated by merging adjacent significantly enriched windows within 1 Kb. To define putative enhancer elements, peak sets of H3K27ac and H3K4me1 were merged, followed by removing regions within 3 Kb from annotated promoters and regions overlapping H3K4me3 peaks.

Analyses of public human single-cell RNA-seq data

Publicly available scRNA-seq read counts from GEO dataset GSE116256 [16] were analyzed using Seurat 3.2.3 package [83]. We used the patient samples with > 300 cells annotated as GMP or GMP-like by the authors. Cells with <200 expressed genes and genes expressed in <3 cells were filtered out, followed by the exclusion of cells with high content of mitochondrial transcripts (> 10% of total reads). Counts across all cells for each sample were normalized using NormalizeData function in Seurat. Individual sub-samples were integrated using Seurat canonical correlation analysis (CCA) method. Integration anchors were determined using FindIntegrationAnchors function and then used in IntegrateData function. We used cell annotations provided in the study to visualize expression of genes of interest in GMP and GMP-like cells using DotPlot function of Seurat.

REFERENCES

1. Ferrando, A. A. & López-Otín, C. Clonal evolution in leukemia. *Nat. Med.* **23**, 1135–1145 (2017).

2. Klco, J. M. *et al.* Functional Heterogeneity of Genetically Defined Subclones in Acute Myeloid Leukemia. *Cancer Cell* **25**, 379–392 (2014).

3. Ding, L. *et al.* Clonal evolution in relapsed acute myeloid leukaemia revealed by whole-genome sequencing. *Nature* **481**, 506–510 (2012).

4. Quek, L. *et al.* Clonal heterogeneity of acute myeloid leukemia treated with the IDH2 inhibitor enasidenib. *Nat. Med.* **24**, 1167–1177 (2018).

5. Takahashi, K. & Tanaka, T. Clonal evolution and hierarchy in myeloid malignancies. *Trends cancer* (2023) doi:10.1016/j.trecan.2023.05.004.

6. Li, S. *et al.* Distinct evolution and dynamics of epigenetic and genetic heterogeneity in acute myeloid leukemia. *Nat. Med.* **22**, 792–799 (2016).

7. Brunetti, L., Gundry, M. C. & Goodell, M. A. DNMT3A in Leukemia. *Csh Perspect Med* **7**, a030320 (2017).

8. Bacher, U. *et al.* Mutations of the TET2 and CBL genes: novel molecular markers in myeloid malignancies. *Ann. Hematol.* **89**, 643–652 (2010).

9. Cenik, B. K. & Shilatifard, A. COMPASS and SWI/SNF complexes in development and disease. *Nat. Rev. Genet.* **22**, 38–58 (2021).

10. Chen, Y. *et al.* MLL2, Not MLL1, Plays a Major Role in Sustaining MLL-Rearranged Acute Myeloid Leukemia. *Cancer Cell* **31**, 755-770.e6 (2017).

11. Cao, F. *et al.* Targeting MLL1 H3K4 Methyltransferase Activity in Mixed-Lineage Leukemia. *Mol. Cell* **53**, 247–261 (2014).

12. Hughes, C. M. *et al.* Menin Associates with a Trithorax Family Histone Methyltransferase Complex and with the Hoxc8 Locus. *Mol. Cell* **13**, 587–597 (2004).

13. Neff, T. *et al.* Polycomb repressive complex 2 is required for MLL-AF9 leukemia. *Proc National Acad Sci* **109**, 5028–5033 (2012).

14. Basheer, F. *et al.* Contrasting requirements during disease evolution identify EZH2 as a therapeutic target in AML. *J Exp Medicine* **216**, 966–981 (2019).

15. Ren, Z. *et al.* A PRC2-Kdm5b axis sustains tumorigenicity of acute myeloid leukemia. *P Natl Acad Sci Usa* **119**, e2122940119 (2022).

16. Galen, P. van *et al.* Single-Cell RNA-Seq Reveals AML Hierarchies Relevant to Disease Progression and Immunity. *Cell* **176**, 1265-1281.e24 (2019).

17. Zeng, A. G. X. *et al.* A cellular hierarchy framework for understanding heterogeneity and predicting drug response in acute myeloid leukemia. *Nat Med* **28**, 1212–1223 (2022).

18. Krivtsov, A. V. *et al.* Transformation from committed progenitor to leukaemia stem cell initiated by MLL–AF9. *Nature* **442**, 818–822 (2006).

19. Meyer, C. *et al.* The MLL recombinome of acute leukemias in 2017. *Leukemia* **32**, 273–284 (2018).

20. Somervaille, T. C. P. & Cleary, M. L. Identification and characterization of leukemia stem cells in murine MLL-AF9 acute myeloid leukemia. *Cancer Cell* **10**, 257–268 (2006).

21. Krivtsov, A. V., Hoshii, T. & Armstrong, S. A. Mixed-Lineage Leukemia Fusions and Chromatin in Leukemia. *Csh Perspect Med* **7**, a026658 (2017).

22. Kuleshov, M. V. *et al.* Enrichr: a comprehensive gene set enrichment analysis web server 2016 update. *Nucleic Acids Res* **44**, W90–W97 (2016).

23. Schuettengruber, B., Bourbon, H.-M., Croce, L. D. & Cavalli, G. Genome Regulation by Polycomb and Trithorax: 70 Years and Counting. *Cell* **171**, 34–57 (2017).

24. Sadreyev, R. I., Yildirim, E., Pinter, S. F. & Lee, J. T. Bimodal quantitative relationships between histone modifications for X-linked and autosomal loci. *Proc. Natl. Acad. Sci.* **110**, 6949–6954 (2013).

25. Margueron, R. & Reinberg, D. The Polycomb complex PRC2 and its mark in life. *Nature* **469**, 343–349 (2011).

26. Bernstein, B. E. *et al.* A Bivalent Chromatin Structure Marks Key Developmental Genes in Embryonic Stem Cells. *Cell* **125**, 315–326 (2006).

27. Bernt, K. M. *et al.* MLL-Rearranged Leukemia Is Dependent on Aberrant H3K79 Methylation by DOT1L. *Cancer Cell* **20**, 66–78 (2011).

28. Machanick, P. & Bailey, T. L. MEME-ChIP: motif analysis of large DNA datasets. *Bioinformatics* **27**, 1696–1697 (2011).

29. Hock, H. & Shimamura, A. ETV6 in hematopoiesis and leukemia predisposition. *Semin. Hematol.* **54**, 98–104 (2017).

30. Endo, A. *et al.* EWSR1/ELF5 induces acute myeloid leukemia by inhibiting p53/p21 pathway. *Cancer Sci.* **107**, 1745–1754 (2016).

31. Duprez, E., Wagner, K., Koch, H. & Tenen, D. G. C/EBPbeta: a major PML-RARA-responsive gene in retinoic acid-induced differentiation of APL cells. *EMBO J.* **22**, 5806–16 (2003).

32. Wang, Q. & Friedman, A. D. CCAAT/enhancer-binding proteins are required for granulopoiesis independent of their induction of the granulocyte colony-stimulating factor receptor. *Blood* **99**, 2776–2785 (2002).

33. Agrawal, S. *et al.* The C/EBPδ tumor suppressor is silenced by hypermethylation in acute myeloid leukemia. *Blood* **109**, 3895–3905 (2007).

34. Dickerson, K. M. *et al.* ZNF384 Fusion Oncoproteins Drive Lineage Aberrancy in Acute LeukemiaRole of ZNF384 Fusions in Lineage Aberrant Leukemia. *Blood Cancer Discov.* **3**, OF1–OF24 (2022).

35. Martino, O. di & Welch, J. S. Retinoic Acid Receptors in Acute Myeloid Leukemia Therapy. *Cancers* **11**, 1915 (2019).

36. Toofan, P. & Wheadon, H. Role of the bone morphogenic protein pathway in developmental haemopoiesis and leukaemogenesis. *Biochem. Soc. Trans.* **44**, 1455–1463 (2016).

37. Cook, B. D., Liu, S. & Evans, T. Smad1 signaling restricts hematopoietic potential after promoting hemangioblast commitment. *Blood* **117**, 6489–97 (2011).

38. Zylbersztejn, F. *et al.* The BMP pathway: A unique tool to decode the origin and progression of leukemia. *Exp Hematol* **61**, 36–44 (2018).

39. Lefort, S. & Maguer-Satta, V. Targeting BMP signaling in the bone marrow microenvironment of myeloid leukemia. *Biochem Soc T* **48**, 411–418 (2020).

40. Yahiro, Y. *et al.* PEG10 counteracts signaling pathways of TGF-β and BMP to regulate growth, motility and invasion of SW1353 chondrosarcoma cells. *J. Bone Miner. Metab.* **37**, 441–454 (2019).

41. Akamatsu, S. *et al.* The Placental Gene PEG10 Promotes Progression of Neuroendocrine Prostate Cancer. *Cell Rep.* **12**, 922–936 (2015).

42. Tang, H. *et al.* Lysyl oxidase drives tumour progression by trapping EGF receptors at the cell surface. *Nat. Commun.* **8**, 14909 (2017).

43. Koth, M. L. *et al.* Canonical Wnt/β-catenin activity and differential epigenetic marks direct sexually dimorphic regulation of Irx3 and Irx5 in developing mouse gonads. *Dev Camb Engl* **147**, (2019).

44. Bonnard, C. *et al.* Mutations in IRX5 impair craniofacial development and germ cell migration via SDF1. *Nat. Genet.* **44**, 709–713 (2012).

45. Sobreira, D. R. *et al.* Extensive pleiotropism and allelic heterogeneity mediate metabolic effects of IRX3 and IRX5. *Science* **372**, 1085–1091 (2021).

46. Zhu, Z. *et al.* Iroquois Homeobox 5 Negatively Regulated by miRNA-147 Promotes the Proliferation, Metastasis, and Invasion by Oral Squamous Cell Carcinoma. *J. Biomed. Nanotechnol.* **17**, 1098–1108 (2021).

47. Zhu, Q. *et al.* IRX5 promotes colorectal cancer metastasis by negatively regulating the core components of the RHOA pathway. *Mol. Carcinog.* **58**, 2065–2076 (2019).

48. Nagel, S., Pommerenke, C., Meyer, C. & MacLeod, R. A. F. The Hematopoietic TALE-Code Shows Normal Activity of IRX1 in Myeloid Progenitors and Reveals Ectopic Expression of IRX3 and IRX5 in Acute Myeloid Leukemia. *Int. J. Mol. Sci.* **23**, 3192 (2022).

49. Olsen, S. N. *et al.* MLL::AF9 degradation induces rapid changes in transcriptional elongation and subsequent loss of an active chromatin landscape. *Mol. Cell* **82**, 1140-1155.e11 (2022).

50. Landrette, S. F. *et al.* Plag1 and Plagl2 are oncogenes that induce acute myeloid leukemia in cooperation with Cbfb-MYH11. *Blood* **105**, 2900–2907 (2005).

51. Yuan, B. *et al.* PTPN3 acts as a tumor suppressor and boosts TGF‐β signaling independent of its phosphatase activity. *EMBO J.* **38**, e99945 (2019).

52. Jenkins, C. R. *et al.* IGF signaling contributes to malignant transformation of hematopoietic progenitors by the MLL-AF9 oncoprotein. *Exp. Hematol.* **40**, 715-723.e6 (2012).

53. Fatrai, S. *et al.* KRASG12V Enhances Proliferation and Initiates Myelomonocytic Differentiation in Human Stem/Progenitor Cells via Intrinsic and Extrinsic Pathways*. *J. Biol. Chem.* **286**, 6061–6070 (2011).

54. Mohedas, A. H. *et al.* Development of an ALK2-Biased BMP Type I Receptor Kinase Inhibitor. *ACS Chem. Biol.* **8**, 1291–1302 (2013).

55. Wang, G. G. *et al.* Quantitative production of macrophages or neutrophils ex vivo using conditional Hoxb8. *Nat. Methods* **3**, 287–293 (2006).

56. Bagger, F. O., Kinalis, S. & Rapin, N. BloodSpot: a database of healthy and malignant haematopoiesis updated with purified and single cell mRNA sequencing profiles. *Nucleic Acids Res.* **47**, D881–D885 (2019).

57. Bottomly, D. *et al.* Integrative analysis of drug response and clinical outcome in acute myeloid leukemia. *Cancer Cell* **40**, 850-864.e9 (2022).

58. Schaefer, E. J. *et al.* BCOR and BCORL1 mutations drive epigenetic reprogramming and oncogenic signaling by unlinking PRC1.1 from target genes. *Blood Cancer Discov.* **3**, bloodcandisc.0115.2021 (2021).

59. Li, M. *et al.* Somatic mutations in the transcriptional corepressor gene BCORL1 in adult acute myelogenous leukemia. *Blood* **118**, 5914–5917 (2011).

60. Wang, D. *et al.* Developmental maturation of the hematopoietic system controlled by a Lin28b-let-7-Cbx2 axis. *Cell Reports* **39**, 110587 (2022).

61. Shima, H. *et al.* Ring1A and Ring1B inhibit expression of Glis2 to maintain murine MOZ-TIF2 AML stem cells. *Blood* **131**, 1833–1845 (2018).

62. Wolfraim, L. A. *et al.* Loss of Smad3 in Acute T-Cell Lymphoblastic Leukemia. *N. Engl. J. Med.* **351**, 552–559 (2004).

63. Le, B. V. *et al.* TGFβR-SMAD3 Signaling Induces Resistance to PARP Inhibitors in the Bone Marrow Microenvironment. *Cell Rep.* **33**, 108221 (2020).

64. Grönroos, E. *et al.* Transforming Growth Factor β Inhibits Bone Morphogenetic Protein-Induced Transcription through Novel Phosphorylated Smad1/5-Smad3 Complexes. *Mol Cell Biol* **32**, 2904–2916 (2012).

65. Vegi, N. M. *et al.* MEIS2 Is an Oncogenic Partner in AML1-ETO-Positive AML. *Cell Rep.* **16**, 498–507 (2016).

66. Oosterwijk, J. G. van *et al.* Hypoxia-induced upregulation of BMX kinase mediates therapeutic resistance in acute myeloid leukemia. *J. Clin. Investig.* **128**, 369–380 (2017).

67. Kishtagari, A., Levine, R. L. & Viny, A. D. Driver mutations in acute myeloid leukemia. *Curr Opin Hematol* **27**, 49–57 (2020).

68. Yang, X., Wong, M. P. M. & Ng, R. K. Aberrant DNA Methylation in Acute Myeloid Leukemia and Its Clinical Implications. *Int J Mol Sci* **20**, 4576 (2019).

69. Network, C. G. A. R. *et al.* Genomic and Epigenomic Landscapes of Adult De Novo Acute Myeloid Leukemia. *N. Engl. J. Med.* **368**, 2059–2074 (2013).

70. Benard, B. A. *et al.* Clonal architecture predicts clinical outcomes and drug sensitivity in acute myeloid leukemia. *Nat. Commun.* **12**, 7244 (2021).

71. Pei, S. *et al.* Monocytic Subclones Confer Resistance to Venetoclax-Based Therapy in Patients with Acute Myeloid Leukemia. *Cancer Discov.* **10**, 536–551 (2020).

72. Morita, K. *et al.* Clonal evolution of acute myeloid leukemia revealed by high-throughput single-cell genomics. *Nat. Commun.* **11**, 5327 (2020).

73. Miles, L. A. *et al.* Single-cell mutation analysis of clonal evolution in myeloid malignancies. *Nature* **587**, 477–482 (2020).

74. Gu, T. *et al.* The disordered N-terminal domain of DNMT3A recognizes H2AK119ub and is required for postnatal development. *Nat. Genet.* **54**, 625–636 (2022).

75. Koya, J. *et al.* DNMT3A R882 mutants interact with polycomb proteins to block haematopoietic stem and leukaemic cell differentiation. *Nat. Commun.* **7**, 10924 (2016).

76. Sykes, D. B. *et al.* Inhibition of Dihydroorotate Dehydrogenase Overcomes Differentiation Blockade in Acute Myeloid Leukemia. *Cell* **167**, 171-186.e15 (2016).

77. Carey, M. F., Peterson, C. L. & Smale, S. T. Chromatin Immunoprecipitation (ChIP). *Cold Spring Harb. Protoc.* **2009**, pdb.prot5279 (2009).

78. Dobin, A. *et al.* STAR: ultrafast universal RNA-seq aligner. *Bioinformatics* **29**, 15–21 (2013).

79. Anders, S., Pyl, P. T. & Huber, W. HTSeq—a Python framework to work with high-throughput sequencing data. *Bioinformatics* **31**, 166–169 (2015).

80. Robinson, M. D., McCarthy, D. J. & Smyth, G. K. edgeR: a Bioconductor package for differential expression analysis of digital gene expression data. *Bioinformatics* **26**, 139–140 (2010).

81. Li, H. & Durbin, R. Fast and accurate short read alignment with Burrows–Wheeler transform. *Bioinformatics* **25**, 1754–1760 (2009).

82. Ramírez, F. *et al.* deepTools2: a next generation web server for deep-sequencing data analysis. *Nucleic Acids Res* **44**, W160–W165 (2016).

83. Hao, Y. *et al.* Integrated analysis of multimodal single-cell data. *Cell* **184**, 3573-3587.e29 (2021).

Figure 1

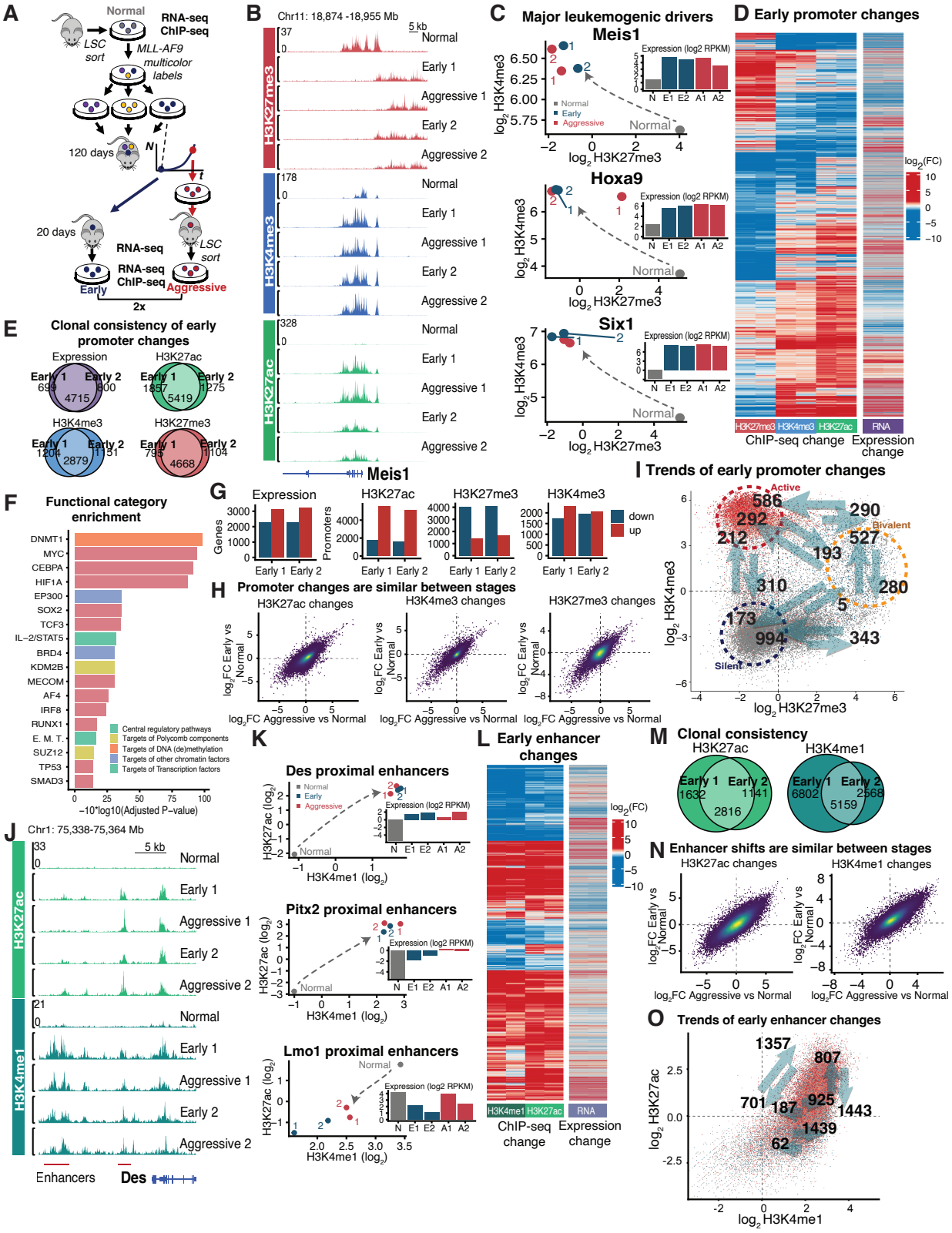
A
Normal
RNA-seq
ChIP-seq
LSC sort
MLL-AF9
multicolor labels
120 days
N
t
20 days
RNA-seq
LSC sort
RNA-seq
ChIP-seq
Early
Aggressive
2x
B
Chr11: 18,874 -18,955 Mb
5 kb
H3K27me3
H3K4me3
H3K27ac
Normal
Early 1
Aggressive 1
Early 2
Aggressive 2
Meis1
C
Major leukemogenic drivers
Meis1
Hoxa9
Six1
Expression (log2 RPKM)
N E1 E2 A1 A2
Normal
Early
Aggressive
log2 H3K4me3
log2 H3K27me3
D
Early promoter changes
log2(FC)
H3K27me3 H3K4me3 H3K27ac RNA
ChIP-seq change
Expression change
E
Clonal consistency of early promoter changes
Expression
H3K27ac
H3K4me3
H3K27me3
Early 1
Early 2
4715
5419
2879
4668
F
Functional category enrichment
DNMT1
MYC
CEBPA
HIF1A
EP300
SOX2
TCF3
IL−2/STAT5
BRD4
KDM2B
MECOM
AF4
IRF8
RUNX1
E. M. T.
SUZ12
TP53
SMAD3
Central regulatory pathways
Targets of Polycomb components
Targets of DNA (de)methylation
Targets of other chromatin factors
Targets of Transcription factors
−10*log10(Adjusted P−value)
G
Expression
H3K27ac
H3K27me3
H3K4me3
Genes
Promoters
down
up
Early 1 Early 2
H
Promoter changes are similar between stages
H3K27ac changes
H3K4me3 changes
H3K27me3 changes
log2FC Early vs Normal
log2FC Aggressive vs Normal
I
Trends of early promoter changes
Active
Bivalent
Silent
586
290
292
527
212
193
310
280
5
173
994
343
log2 H3K4me3
log2 H3K27me3
J
Chr1: 75,338-75,364 Mb
5 kb
H3K27ac
H3K4me1
Normal
Early 1
Aggressive 1
Early 2
Aggressive 2
Enhancers
Des
K
Des proximal enhancers
Pitx2 proximal enhancers
Lmo1 proximal enhancers
H3K27ac (log2)
H3K4me1 (log2)
L
Early enhancer changes
log2(FC)
H3K4me1 H3K27ac RNA
ChIP-seq change
Expression change
M
Clonal consistency
H3K27ac
H3K4me1
Early 1
Early 2
1632
1141
2816
6802
2568
5159
N
Enhancer shifts are similar between stages
H3K27ac changes
H3K4me1 changes
log2FC Early vs Normal
log2FC Aggressive vs Normal
O
Trends of early enhancer changes
1357
807
701
187
925
1443
1439
62
log2 H3K27ac
log2 H3K4me1

Figure 2

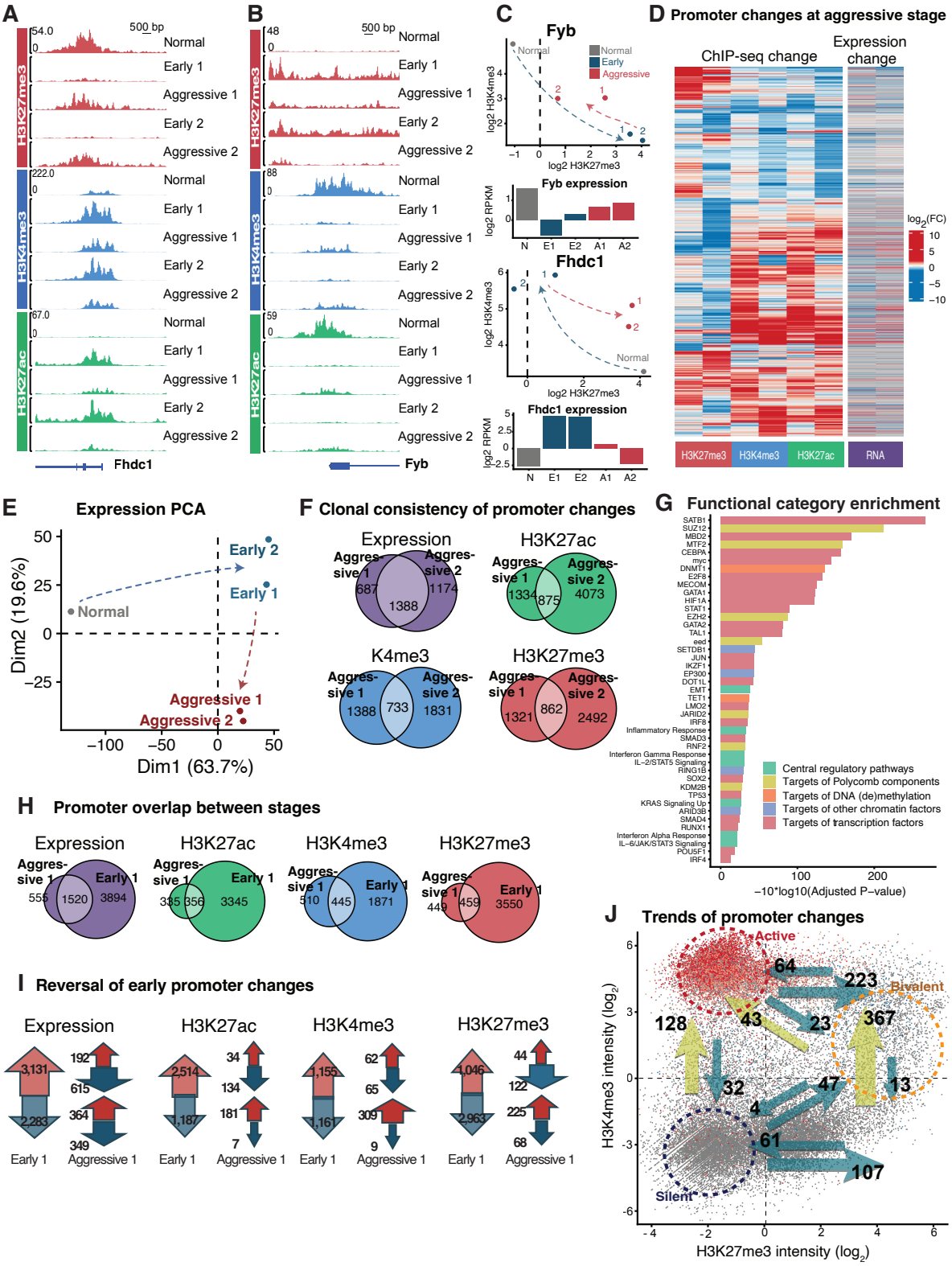
A
B
C
D Promoter changes at aggressive stage
H3K27me3
H3K4me3
H3K27ac
Normal
Early 1
Aggressive 1
Early 2
Aggressive 2
500 bp
Fhdc1
Fyb
Fyb expression
Fhdc1 expression
log2 H3K4me3
log2 H3K27me3
log2 RPKM
ChIP-seq change
Expression change
log2(FC)
RNA
E Expression PCA
Dim1 (63.7%)
Dim2 (19.6%)
F Clonal consistency of promoter changes
Expression
H3K27ac
K4me3
H3K27me3
Aggressive 1
Aggressive 2
G Functional category enrichment
Central regulatory pathways
Targets of Polycomb components
Targets of DNA (de)methylation
Targets of other chromatin factors
Targets of transcription factors
−10*log10(Adjusted P−value)
H Promoter overlap between stages
I Reversal of early promoter changes
J Trends of promoter changes
Active
Bivalent
Silent
H3K4me3 intensity (log2)
H3K27me3 intensity (log2)

Figure 3

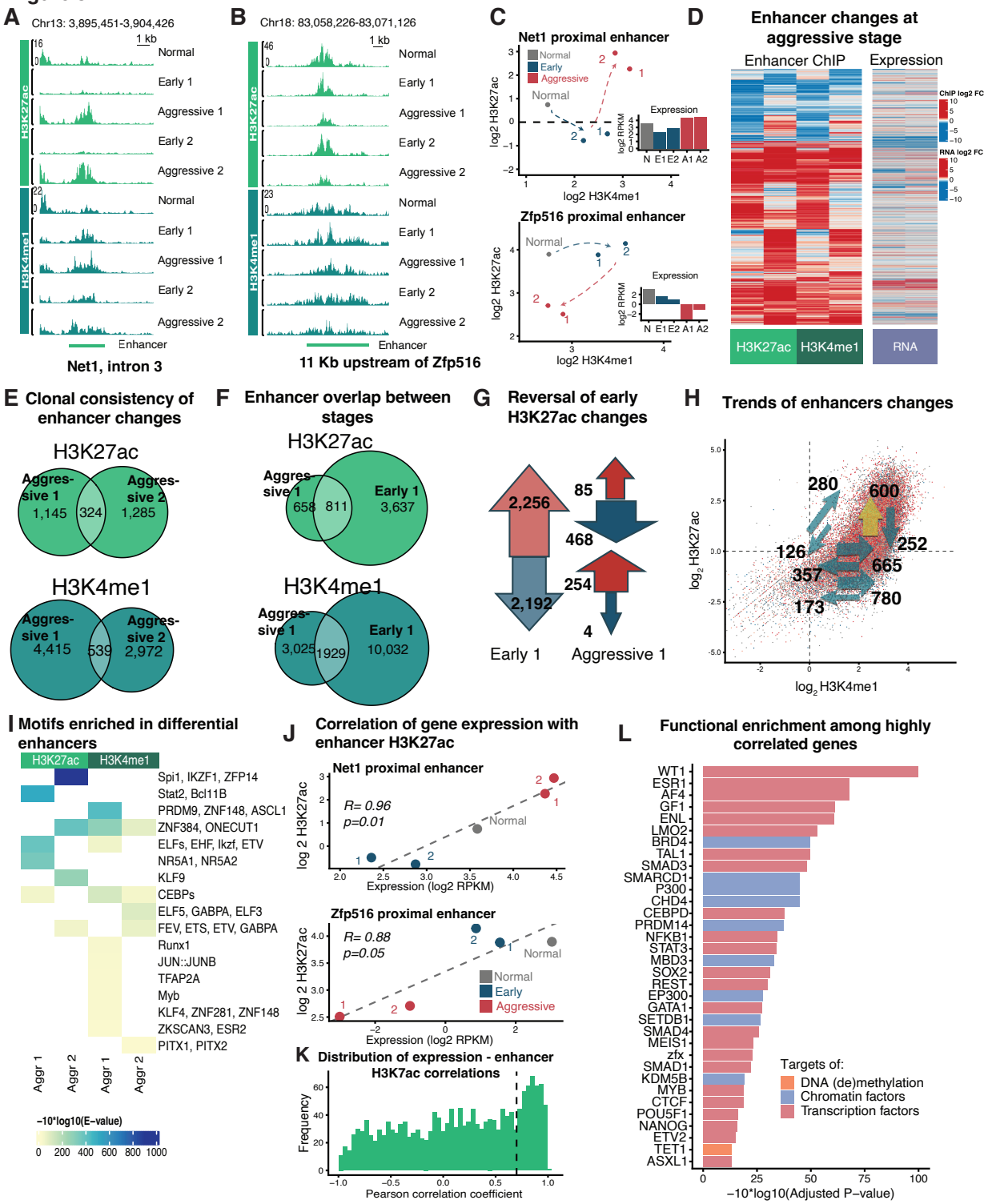
A
Chr13: 3,895,451-3,904,426
1 kb
H3K27ac
H3K4me1
Normal
Early 1
Aggressive 1
Early 2
Aggressive 2
Enhancer
Net1, intron 3
B
Chr18: 83,058,226-83,071,126
11 Kb upstream of Zfp516
C
Net1 proximal enhancer
Normal
Early
Aggressive
log2 H3K27ac
log2 H3K4me1
Expression
log2 RPKM
N E1 E2 A1 A2
Zfp516 proximal enhancer
D
Enhancer changes at aggressive stage
Enhancer ChIP
Expression
ChIP log2 FC
RNA log2 FC
H3K27ac
H3K4me1
RNA
E Clonal consistency of enhancer changes
H3K27ac
Aggres-sive 1
1,145
324
Aggres-sive 2
1,285
H3K4me1
Aggres-sive 1
4,415
539
Aggres-sive 2
2,972
F Enhancer overlap between stages
H3K27ac
Aggres-sive 1
658
811
Early 1
3,637
H3K4me1
Aggres-sive 1
3,025
1929
Early 1
10,032
G Reversal of early H3K27ac changes
2,256
85
468
254
2,192
4
Early 1
Aggressive 1
H Trends of enhancers changes
280
600
126
252
357
665
173
780
log2 H3K27ac
log2 H3K4me1
I Motifs enriched in differential enhancers
H3K27ac
H3K4me1
Spi1, IKZF1, ZFP14
Stat2, Bcl11B
PRDM9, ZNF148, ASCL1
ZNF384, ONECUT1
ELFs, EHF, Ikzf, ETV
NR5A1, NR5A2
KLF9
CEBPs
ELF5, GABPA, ELF3
FEV, ETS, ETV, GABPA
Runx1
JUN::JUNB
TFAP2A
Myb
KLF4, ZNF281, ZNF148
ZKSCAN3, ESR2
PITX1, PITX2
Aggr 1
Aggr 2
Aggr 1
Aggr 2
−10*log10(E−value)
0 200 400 600 800 1000
J Correlation of gene expression with enhancer H3K27ac
Net1 proximal enhancer
R= 0.96
p=0.01
Normal
log 2 H3K27ac
Expression (log2 RPKM)
Zfp516 proximal enhancer
R= 0.88
p=0.05
Normal
Early
Aggressive
K Distribution of expression - enhancer H3K7ac correlations
Frequency
Pearson correlation coefficient
L Functional enrichment among highly correlated genes
WT1
ESR1
AF4
GF1
ENL
LMO2
BRD4
TAL1
SMAD3
SMARCD1
P300
CHD4
CEBPD
PRDM14
NFKB1
STAT3
MBD3
SOX2
REST
EP300
GATA1
SETDB1
SMAD4
MEIS1
zfx
SMAD1
KDM5B
MYB
CTCF
POU5F1
NANOG
ETV2
TET1
ASXL1
Targets of:
DNA (de)methylation
Chromatin factors
Transcription factors
−10*log10(Adjusted P−value)

Figure 4

A Filtering by consistency of promoter changes

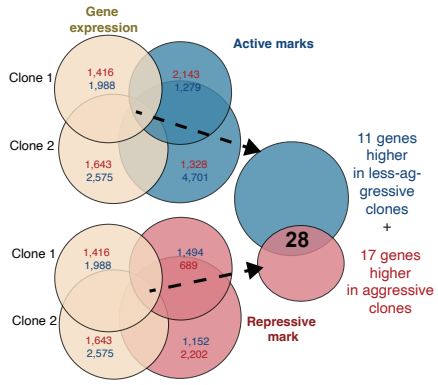

B Consistent changes of core genes

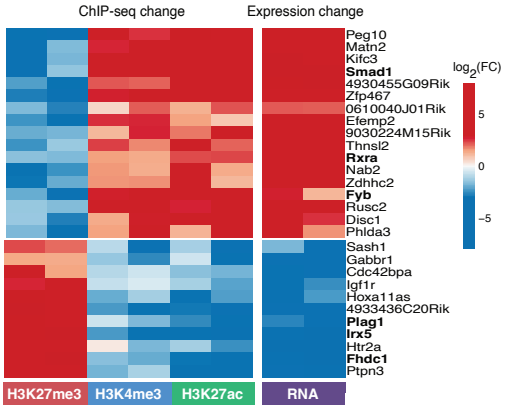

C Stage-specific degrees of activation

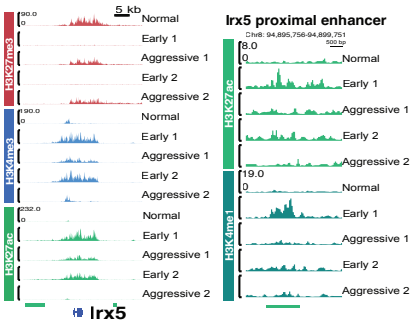

D

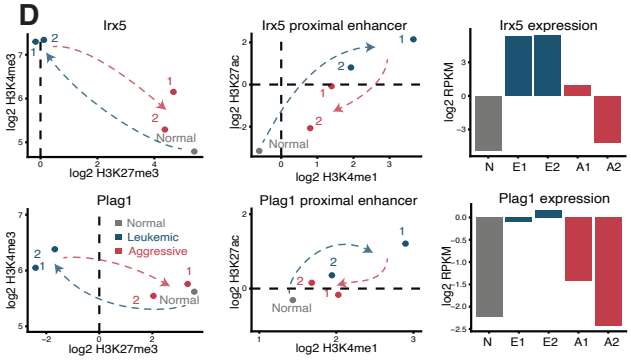

E Stage-specific degrees of repression

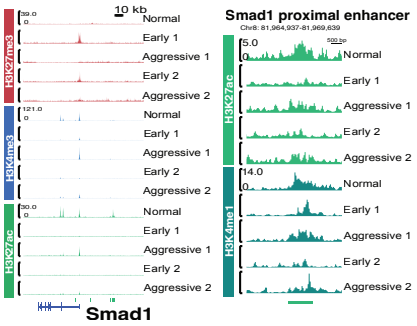

F

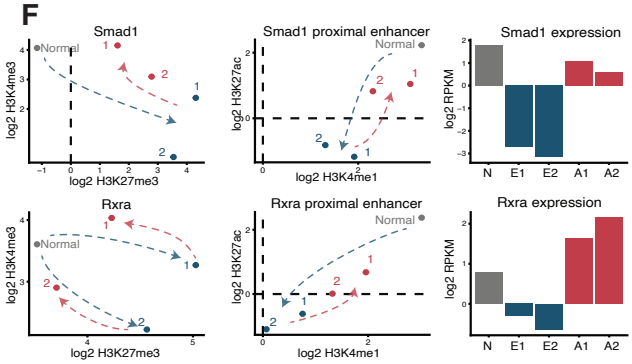

G Promoter overlap between stages

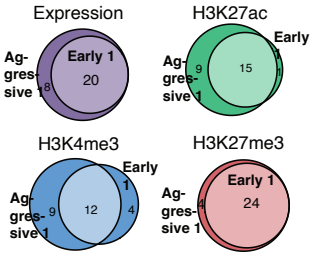

H Reversal of early promoter changes

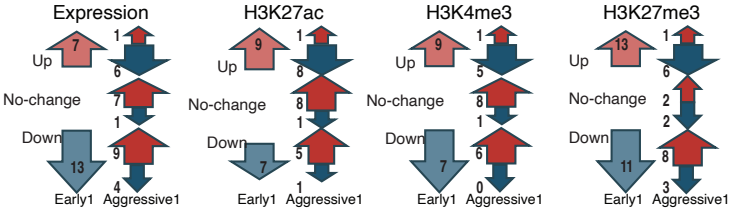

Figure 5

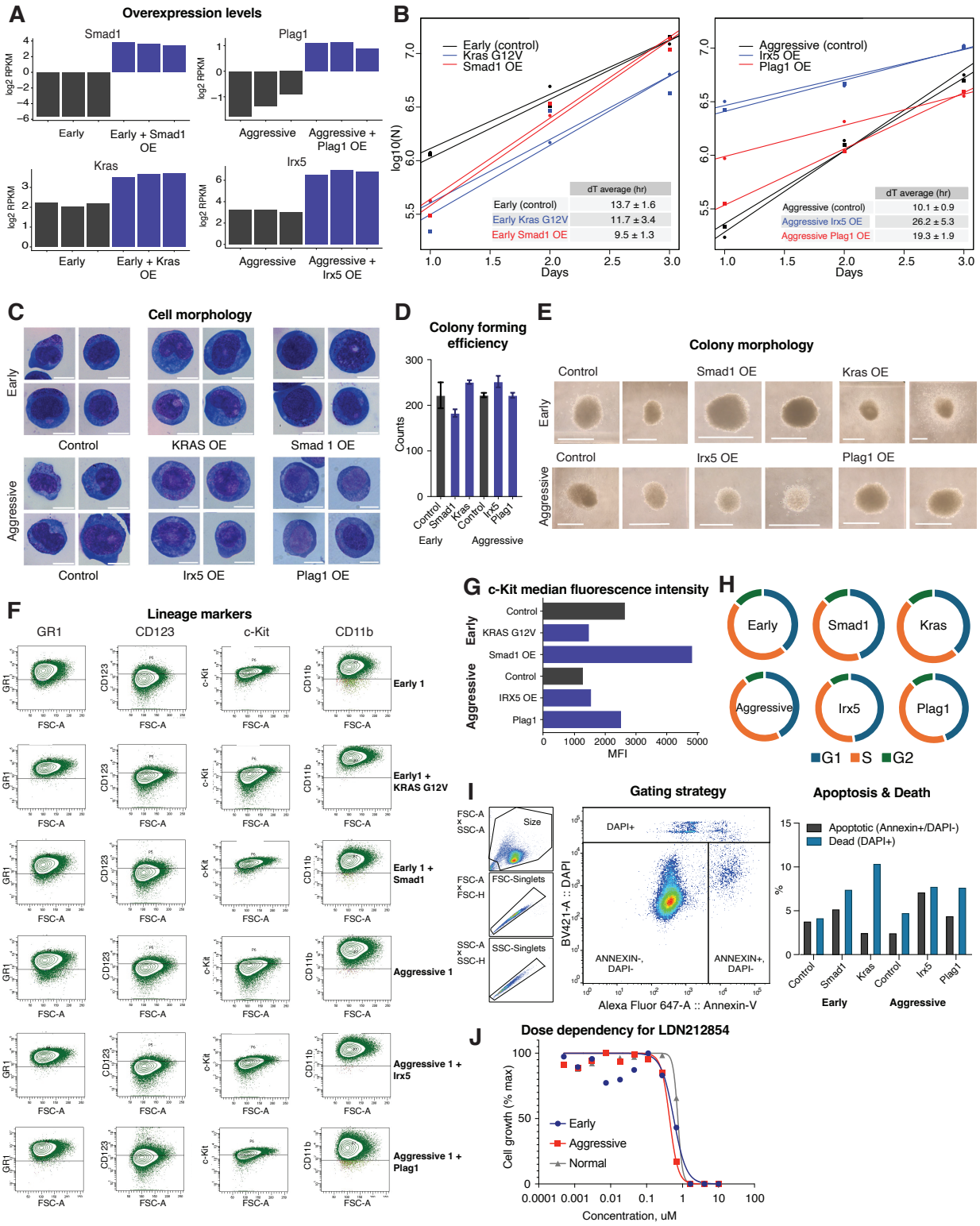
A
Overexpression levels
Smad1
Plag1
Kras
Irx5
log2 RPKM
Early
Early + Smad1 OE
Aggressive
Aggressive + Plag1 OE
Early + Kras OE
Aggressive + Irx5 OE
B
Early (control)
Kras G12V
Smad1 OE
Aggressive (control)
Irx5 OE
Plag1 OE
log10(N)
Days
dT average (hr)
Early (control) 13.7 ± 1.6
Early Kras G12V 11.7 ± 3.4
Early Smad1 OE 9.5 ± 1.3
Aggressive (control) 10.1 ± 0.9
Aggressive Irx5 OE 26.2 ± 5.3
Aggressive Plag1 OE 19.3 ± 1.9
C
Cell morphology
Early
Aggressive
Control
KRAS OE
Smad 1 OE
Irx5 OE
Plag1 OE
D
Colony forming efficiency
Counts
Control
Smad1
Kras
Control
Irx5
Plag1
Early
Aggressive
E
Colony morphology
Control
Smad1 OE
Kras OE
Irx5 OE
Plag1 OE
F
Lineage markers
GR1
CD123
c-Kit
CD11b
FSC-A
Early 1
Early1 + KRAS G12V
Early 1 + Smad1
Aggressive 1
Aggressive 1 + Irx5
Aggressive 1 + Plag1
G
c-Kit median fluorescence intensity
Control
KRAS G12V
Smad1 OE
Control
IRX5 OE
Plag1
MFI
H
Early
Smad1
Kras
Aggressive
Irx5
Plag1
G1
S
G2
I
Gating strategy
FSC-A x SSC-A
Size
FSC-A x FSC-H
FSC-Singlets
SSC-A x SSC-H
SSC-Singlets
DAPI+
ANNEXIN-, DAPI-
ANNEXIN+, DAPI-
BV421-A :: DAPI
Alexa Fluor 647-A :: Annexin-V
Apoptosis & Death
Apoptotic (Annexin+/DAPI-)
Dead (DAPI+)
%
Control
Smad1
Kras
Control
Irx5
Plag1
Early
Aggressive
J
Dose dependency for LDN212854
Cell growth (% max)
Early
Aggressive
Normal
Concentration, uM

Figure 6

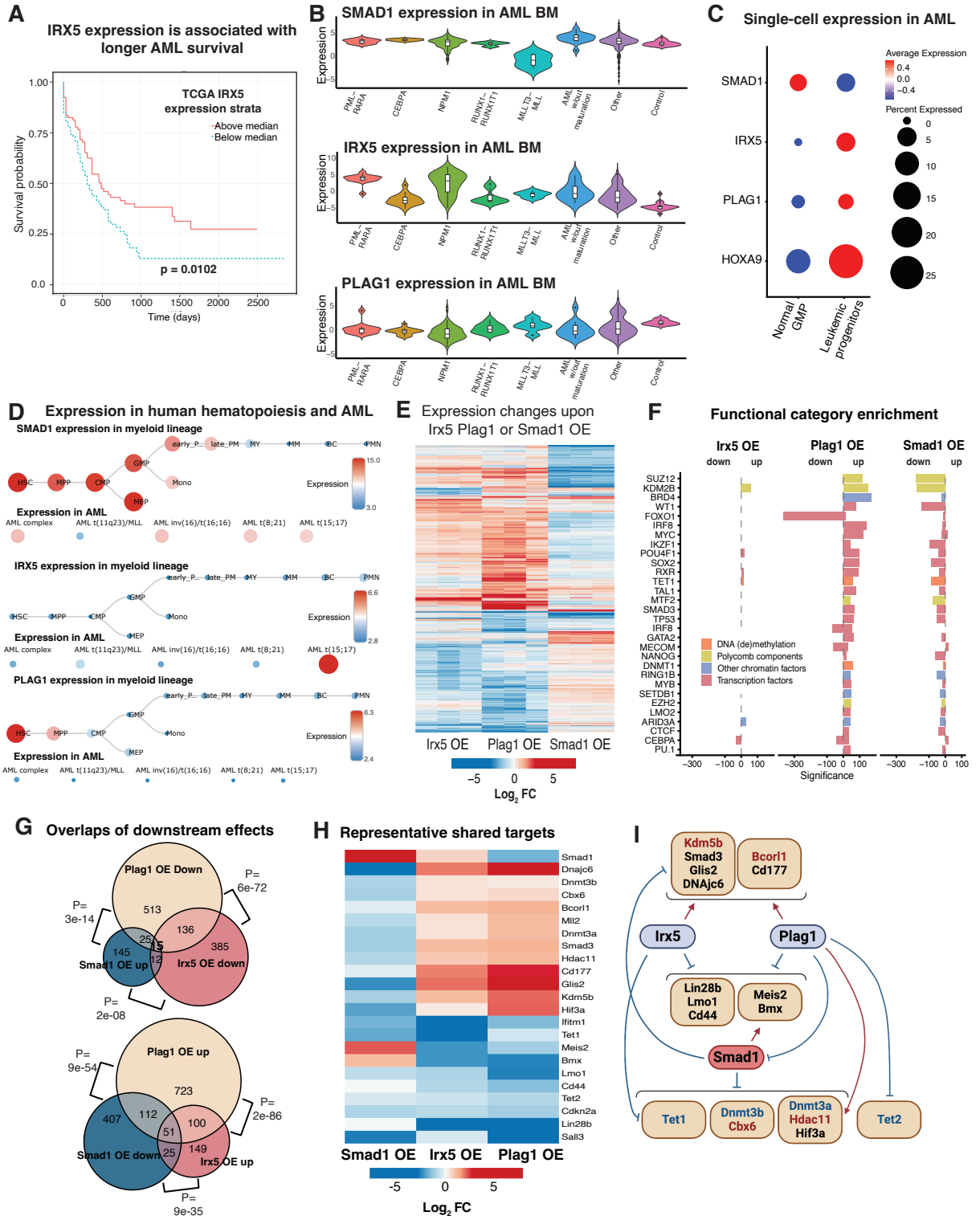
A
IRX5 expression is associated with longer AML survival
TCGA IRX5 expression strata
Above median
Below median
Survival probability
Time (days)
p = 0.0102
B
SMAD1 expression in AML BM
IRX5 expression in AML BM
PLAG1 expression in AML BM
Expression
PML-RARA
CEBPA
NPM1
RUNX1-RUNX1T1
MLLT3-MLL
AML w/out maturation
Other
Control
C
Single-cell expression in AML
Average Expression
Percent Expressed
SMAD1
IRX5
PLAG1
HOXA9
Normal GMP
Leukemic progenitors
D
Expression in human hematopoiesis and AML
SMAD1 expression in myeloid lineage
IRX5 expression in myeloid lineage
PLAG1 expression in myeloid lineage
Expression in AML
HSC
MPP
CMP
GMP
MEP
Mono
MY
MM
BC
PMN
AML complex
AML t(11q23)/MLL
AML inv(16)/t(16;16)
AML t(8;21)
AML t(15;17)
E
Expression changes upon Irx5 Plag1 or Smad1 OE
Irx5 OE
Plag1 OE
Smad1 OE
Log2 FC
F
Functional category enrichment
Irx5 OE
Plag1 OE
Smad1 OE
down
up
DNA (de)methylation
Polycomb components
Other chromatin factors
Transcription factors
Significance
G
Overlaps of downstream effects
Plag1 OE Down
Smad1 OE up
Irx5 OE down
Plag1 OE up
Smad1 OE down
Irx5 OE up
P= 3e-14
P= 6e-72
P= 2e-08
P= 9e-54
P= 2e-86
P= 9e-35
H
Representative shared targets
Smad1
Dnajc6
Dnmt3b
Cbx6
Bcorl1
Mll2
Dnmt3a
Smad3
Hdac11
Cd177
Glis2
Kdm5b
Hif3a
Ifitm1
Tet1
Meis2
Bmx
Lmo1
Cd44
Tet2
Cdkn2a
Lin28b
Sall3
Smad1 OE
Irx5 OE
Plag1 OE
Log2 FC
I
Kdm5b Smad3 Glis2 DNAjc6
Bcorl1 Cd177
Irx5
Plag1
Lin28b Lmo1 Cd44
Meis2 Bmx
Smad1
Tet1
Dnmt3b Cbx6
Dnmt3a Hdac11 Hif3a
Tet2